Huang *et al. Energy Mater* 2024;4:400030
DOI: 10.20517/energymater.2023.83

Energy Materials

Review

Open Access

Engineering of lithiophilic hosts for stable lithium metal anodes

Lianzhan Huang[1,#], Wei Li[2,#], Zhiming Cui[1,*]

[1]School of Chemistry and Chemical Engineering, South China University of Technology, Guangzhou 510641, Guangdong, China.
[2]The Technology Innovation Centre, Guangdong Electric Power Development Co., LTD, Guangzhou 510620, Guangdong, China.
[#]Authors contributed equally.

[*]**Correspondence to:** Prof. Zhiming Cui, School of Chemistry and Chemical Engineering, South China University of Technology, No.381, Wushan Road, Tianhe District, Guangzhou 510641, Guangdong, China. E-mail: zmcui@scut.edu.cn

How to cite this article: Huang L, Li W, Cui Z. Engineering of lithiophilic hosts for stable lithium metal anodes. *Energy Mater* 2024;4:400030. https://dx.doi.org/10.20517/energymater.2023.83

Received: 24 Oct 2023 **First Decision:** 17 Jan 2024 **Revised:** 25 Jan 2024 **Accepted:** 26 Mar 2024 **Published:** 8 Apr 2024

Academic Editor: Jiaqi Huang **Copy Editor:** Dong-Li Li **Production Editor:** Dong-Li Li

Abstract

Lithium (Li^0) metal has been deemed the desired anode for the future of cutting-edge rechargeable Li batteries benefiting from its lowest reduction potential and ultrahigh theoretical specific capacity. Nevertheless, the large-scale applications of Li metal batteries are restricted by scattered Li dendrite formation and uncontrollable volume expansion. To address these issues, a currently prevalent measure is to use structured lithiophilic hosts for Li metal. The enhanced lithiophilicity of hosts is significant for regulating the Li nucleation barrier. By virtue of these lithiophilic measures, the Li nucleation sites will be well controlled and the Li plating layer will be more stable. Through this article, we classified various lithiophilic hosts and described their applications for Li metal batteries, including heteroatom-doping carbon, lithiophilic-material loading hosts and gradient skeletons. We discussed the inherent advantages and lithophilic mechanisms of these hosts on optimizing the lithophilic properties and analyzed various factors that induced the formation of dendrite Li. Moreover, the review outlines the current challenges and perspectives for Li metal anodes, and some understanding of the lithiophilic chemistry is given.

Keywords: Lithiophilic host, lithium metal anode, lithiophilic mechanism

INTRODUCTION

Lithium-ion batteries (LIBs), one of the most widely used electrochemical energy storage devices, have brought much convenience to modern life[1-5]. After SONY successfully commercialized LIBs, numerous

studies focused on improving their performance and quality. Currently, they have been successfully employed in mobile phones, laptops, electric vehicles[6-10], *etc*. However, LIBs with relatively low theoretical capacity (372 mAh·g^{-1}) cannot meet the need of fast-growing electric equipment, such as electric vehicles[11-13]. As we know, lithium metal (Li^0) as the anode has the lowest reduction potential (-3.04 V *vs*. the standard hydrogen electrode) and ultrahigh theoretical specific capacity (3,860 mAh·g^{-1}), which has attracted extensive attention during the past years[14-18]. As Li metal batteries (LMBs) gather pace, such as Li-Air batteries[19-21] and Li-Sulfur (S) batteries[22-24], Li metal anodes have no doubt taken the crown of the most potential electrode materials.

Although Li anodes have advantages, the safety and durability among these issues have restricted their practical application in LMBs[25-28]. First, the formation of Li dendrites would cause internal short circuits of LMBs[29-31]. Second, the abundant Li dendrites also lead to volume change of batteries[32-34]. Third, the parasitic reactions will generate plenty of "dead Li" and increase the thickness of solid electrolyte interface (SEI)[35,36]. To deal with these problems, people have taken various methods, including electrolyte additives[37-39], solid state electrolytes (SSEs)[40-43], and interface protection layers[14,44-46]. However, Li metal, as a metallic electrode, undergoes the deposition/dissolution of Li, and its deposition morphology is highly related to the initial nucleation and growth stages of Li metal seeds[47,48]. The above-mentioned strategies are not always secure when suppressing the Li dendrites. For instance, optimizing electrolyte composition will contribute to generating a sturdy SEI layer[49,50], which effectively prevents further side reactions. Indeed, these methods have exhibited improved cycling life. However, once Li metal dendrites are generated, the native SEI film will be destroyed and side reactions will inevitably occur in the battery system. Moreover, SSEs with satisfied mechanical strength can also help to inhibit volume expansion. However, the grain boundaries of SSEs are the lodging where Li metal tends to grow inside during the plating process; this ultimately induces a short circuit of batteries[51]. Some researchers have observed the evolution of Li metal deposition in situ, which provides a guide for designing dendrite-free composite anodes. For example, the concentration change of the cell with an interelectrode length was described by Rosso *et al.* through a diffusion formula for the boundary condition[52], expressed as

$$\frac{\partial C}{\partial x}(x) = \frac{J\mu_a}{eD(\mu_a + \mu_{Li^+})} \tag{1}$$

where J refers to the intrinsic current density of Li anodes, and e represents the charge of electrons, and D corresponds to the ambipolar diffusion constant. μ_a is mobility of counteranions, and μ_{Li+} is mobility of Li-ions (Li$^+$). When the $\frac{\partial C}{\partial x}(x) < 2\frac{C_0}{L}$ (L means the inner electrode distance and C_0 represents the original electrode concentration), the ionic concentration at an anode will be stable, which means the concentration gradient is constant and the deposited Li metal will be more homogeneous. However, if $\frac{\partial C}{\partial x}(x) > 2\frac{C_0}{L}$, the ionic concentration at anodes will fall to zero at "Sand's Time" (τ), which can be calculated according to "Sand's Equation", denoted as

$$\tau = \pi D \frac{e^2 C_0^2 (\mu_a + \mu_{Li^+})^2}{4J^2 \mu_a^2} \tag{2}$$

Based on this equation, an efficient strategy to restrain the growth of Li dendrite is decreasing the effective current density of Li anodes. However, simply increasing the specific surface area of the Li host cannot completely solve uneven Li deposition. When applying lithiophobic materials for the anode host, the nucleation overpotential is still basically unchanged, and even the local current is greatly reduced. Thus, the overpotential of anabatic nucleation leads to large Li$^+$ resistance and unstable thermodynamics at the anode

surface, which further results in a chaotic and loosened deposition layer[53,54]. The overpotential of Li nucleation can be significantly lowered by giving Li hosts with lithiophilicity, thereby ensuring even Li nucleation at the initial stage and laying a good foundation to develop compact Li layers[55,56]. Besides, the even Li deposit layer may also assure the integrity of the SEI, reducing the generation of "dead Li"[35,57]. The study findings on lithiophilic hosts in Li metal anodes during the past few years are presented in this paper. In terms of the categories of different lithiophilic hosts [Figure 1] and their interaction mechanisms, the characteristics of various lithiophilic techniques for improving Li deposition are discussed.

WELL-DESIGNED HOSTS FOR HOMOGENEOUS LI DEPOSITION

The "hostless" feature of metallic Li renders its deposition morphology random, and the low surface energy and high diffusion barrier causes Li deposits to evolve into dendrites, which will puncture the separator so as to cause the battery failure[58-60]. Moreover, electrochemical reduction of Li^+ is not at the bulk Li but is always confined at the vicinity of the electrode, so the Li deposition kinetics is relatively sluggish. All of these factors hinder the stable operation of Li metal anodes in practical working situations. According to the "Sand's time" equation, the intrinsic current density of Li electrodes and transference numbers of Li^+ are both key parameters to manage dendrite growth. Researchers have designed numerous composite Li anodes through high specific surface hosts[61], which can lower the local current density and successfully control dendrite growth. Configuration of structural Li anodes is usually realized by integrating Li metal into the host by melting[62-65], pre-deposition[66-68], and mechanical rolling[3,69,70]. Besides, the lithiophilicity of hosts is significant, including surface chemical properties and entire structure of the host, which determines the deposition result of the Li metal in the framework[71,72]. So, endowing Li hosts with rational structures and different functional groups is regarded as an effective method to improve cycle stability of the Li metal anodes.

Heteroatom doping of lithium hosts

Due to the unique structure of sp^2 carbon in the carbon materials, many kinds of non-metallic elements have been used as dopants to form the doped structure on the carbon ring[73] [Figure 2A]. Adjusting the kind and number of heteroatoms can change the electronic properties of these heteroatom-doped carbons, which endows them with more unique chemical properties. These heteroatom-doped carbon materials are widely used in the energy storage field [Figure 2B and C]. As mentioned above, the effective current density could be vastly attenuated by Li hosts with enough inner space. However, the mismatch between Li and host still exists, which means the uniform Li nucleation is difficult. Heteroatom doping can be adopted to enhance the Li affinity of the host and facilitate uniform Li deposition, because its surface chemistry highly influences the inchoate morphology of Li. Among these materials, heteroatom-doped carbon is the most widely used lithiophilic framework. It is currently recognized that heteroatom doping increases the defect number of the host to offer more interaction sites, so the Li affinity is improved[74].

Unfortunately, the underlying reasons for the lithiophilicity of these hosts remained ambiguous for a long time. Recently, the lithiophilic property of doping sites was clarified by Chen *et al.*[75]. They consider that electronegativity, local dipole, and charge transfer account for the lithiophilicity of doping sites. The electronegativity of the doping site is significant for Li nucleation because it can drive Li^+ closer to the host to form chemical bonds and complete the charge transfer process [Figure 2D]. Moreover, they summarized the binding energy of different heteroatom-doped carbons toward Li [Figure 2E]. Some of the more electronegative heteroatoms [oxygen (O), Nitrogen (N), phosphorus (P), *etc.*] are generally doped into the carbon material to improve its lithiophilicity. Single heteroatom doping, dual-doping, and anchoring metal atoms on the doped host are three major approaches to constructing an improved Li host to achieve a LMB with a long lifespan. Some of the lithiophilic hosts with different heteroatom doping and their corresponding electrochemical performances are presented in Table 1.

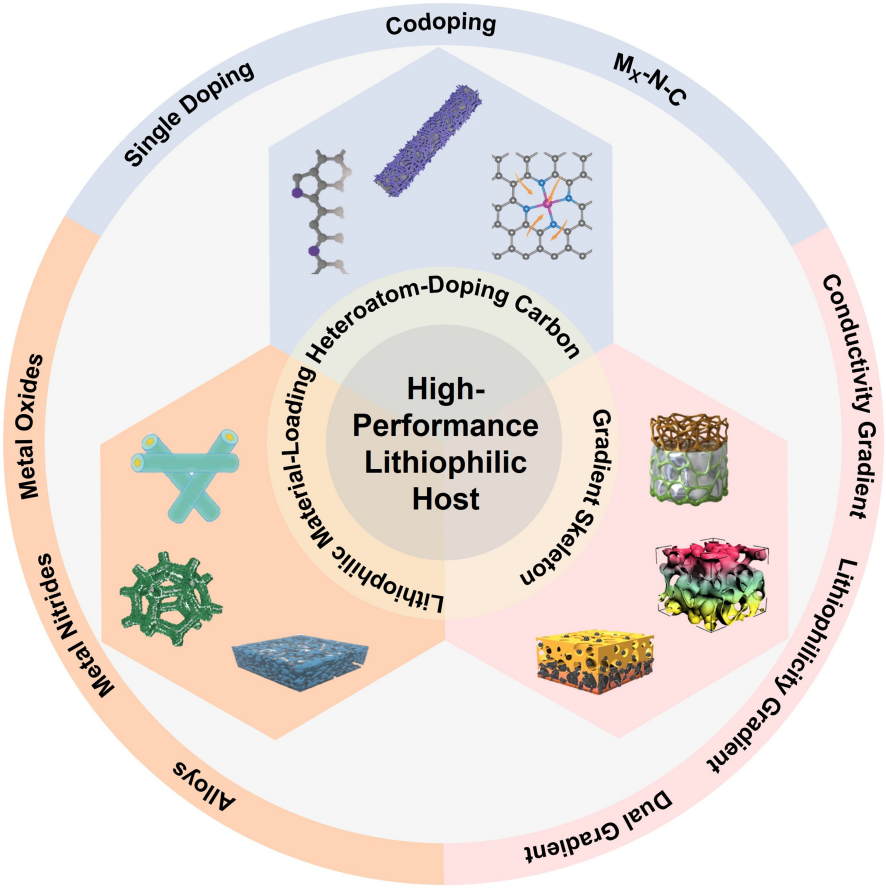

Figure 1. Classification and summary of lithiophilic hosts.

Single heteroatom doping

N-doped carbon substrates are widely used as lithiophilic hosts to guide regular Li deposition[76,77]. In these doped structures, N-containing species such as pyrrolic and pyridinic nitrogen, exhibit strong binding energy with Li^+. This is because these nitrogenous species belonging to Lewis base sites can interact with Li^+, consequently guiding uniform Li nucleation. A modified graphene containing nitrogen (NG) is proposed by Zhang *et al.* to achieve dendrite-free Li[78] [Figure 3A]. As shown in Figure 3B, compared to copper (Cu) and graphene electrodes, the NG electrode with pyrrolic and pyridinic nitrogen functional groups showed a reduced overpotential, which indicates the NG matrix is highly lithiophilic. Additionally, the large specific area of the NG scaffold reduced local current density to effectively postpone the time of dendrite formation. According to the scanning electron microscopy (SEM) characterization, Li deposition on the NG matrix was smoother and denser with dendrite-free morphology, while loose and heterogeneous deposition furiously accumulated on the Cu foil. With the test condition of 1 $mA{\cdot}cm^{-2}$ and 1 $mAh{\cdot}cm^{-2}$, the coulombic efficiency (CE) of the NG electrode retained 98% after 200 cycles, but the control group fluctuated wildly and fell below 70% at 70 cycles. The electrochemical performance results and morphology characterization demonstrated that introducing nitrogen atoms into the graphene scaffold can improve its Li affinity greatly and prolong the battery cycling life.

Table 1. A summary of electrochemical performance of different lithiophilic hosts with heteroatom doping strategy

Li Hosts	Materials	Li/Cu cells (current density; area capacity; cycle number; CE)	Symmetrical cells (current density; area capacity; cycle time)	$LiFePO_4$ full cells (discharge current; cycle number; capacity retention)	Ref.
NG	Nitrogen-doped graphene	1 $mA·cm^{-2}$; 1 $mAh·cm^{-2}$; 200 cycles; 98% 1 $mA·cm^{-2}$; 2 $mAh·cm^{-2}$; 50 cycles; 98%	1 $mA·cm^{-2}$; 0.042 $mAh·cm^{-2}$; 300 h		[78]
CB@rGO	N-doped hollow porous bowl-like hard carbon/ reduced graphene nanosheets	1 $mA·cm^{-2}$; 1 $mAh·cm^{-2}$; 600 cycles; 98%	1 $mA·cm^{-2}$; 1 $mAh·cm^{-2}$; 600 h	1 C; 200 cycles	[76]
DLCTs	N-doped carbon tubes	3 $mA·cm^{-2}$; 3 $mAh·cm^{-2}$; 300 cycles; 99.3%	2 $mA·cm^{-2}$; 2 $mAh·cm^{-2}$; 1,200 h 5 $mA·cm^{-2}$; 5 $mAh·cm^{-2}$; 200 h	1 C; 300 cycles; 88.6% 5 C; 300 cycles; 85.2%	[77]
NGCFs	Nitrogen-doped graphitic carbon foams	2 $mA·cm^{-2}$; 2 $mAh·cm^{-2}$; 300 cycles; 99.6% 2 $mA·cm^{-2}$; 6 $mAh·cm^{-2}$; 150 cycles; 99.4% 2 $mA·cm^{-2}$; 8 $mAh·cm^{-2}$; 140 cycles; 99.1%	2 $mA·cm^{-2}$; 1 $mAh·cm^{-2}$; 1,200 h 3 $mA·cm^{-2}$; 1 $mAh·cm^{-2}$; 600 h	0.5 C; 200 cycles; 90%	[79]
3DP-NC	N-doped carbon framework	1 $mA·cm^{-2}$; 10 $mAh·cm^{-2}$; 100 cycles; 97.9%	10 $mA·cm^{-2}$; 2 $mAh·cm^{-2}$; 150 h		[80]
NPCC	N, P codoped carbon cloth	3 $mA·cm^{-2}$; 10 $mAh·cm^{-2}$; 100 cycles; 97.9%	3 $mA·cm^{-2}$; 600 h 5 $mA·cm^{-2}$; 240 h	2 C; 600 cycles; 86.6%	[82]
NS-CP	Nitrogen and sulfur codoped carbon paper	1 $mA·cm^{-2}$; 1 $mAh·cm^{-2}$; 100 cycles; 99.5%	0.5 $mA·cm^{-2}$; 1 $mAh·cm^{-2}$; 600 h 1 $mA·cm^{-2}$; 1 $mAh·cm^{-2}$; 500 h	2 C; 200 cycles	[84]
OBHcCs	Oxygen, boron codoped honeycomb carbon skeleton	0.5 $mA·cm^{-2}$; 1 $mAh·cm^{-2}$; 220 cycles; 97.7% 1 $mA·cm^{-2}$; 1 $mAh·cm^{-2}$; 150 cycles; 97.3% 2 $mA·cm^{-2}$; 1 $mAh·cm^{-2}$; 110 cycles; 96.1%	0.5 $mA·cm^{-2}$; 1 $mAh·cm^{-2}$; 1,400 h 1 $mA·cm^{-2}$; 1 $mAh·cm^{-2}$; 700 h	0.5 C; 500 cycles; 84.6%	[85]
CoNC	N-doped carbon structure	2 $mA·cm^{-2}$; 2 $mAh·cm^{-2}$; 400 cycles; 99.2%		1 C; 340 cycles; 98.4%	[88]
SANi-NG	Ni metals on doped graphene	0.5 $mA·cm^{-2}$; 1 $mAh·cm^{-2}$; 250 cycles; 98.45% 2 $mA·cm^{-2}$; 1 $mAh·cm^{-2}$; 150 cycles; 97.7%			[87]
SAM@NG	Single-atom on doped graphene	1 $mA·cm^{-2}$; 1 $mAh·cm^{-2}$; 280 cycles; 99.0%		1 C; 210 cycles; 90%	[86]

CE: Coulombic efficiency; NG: graphene containing nitrogen; CB@rGO: N-doped hollow bowl-like carbon loaded on rGO; DLCTs: N-doped carbon tubes; NGCFs: N-doped graphitic carbon foams; 3DP-NC: N-doped carbon host; NPCC: N, P codoped carbon cloth; NS-CP: N and S codoped carbon paper; OBHcCs: B and O bi-functionalized carbon current collectors; CoNC: Co atoms anchored in the N-doped carbon structure; SANi-NG: single Ni atoms supported on nitrogen.

Except for the layered graphene, a lightweight N-doped graphitic carbon foam (NGCF) electrode with three-dimension (3D) crosslinking structures was also employed to guide uniform Li deposition[79]. The rich nitrogenous species formed on carbon rings ensure the foam has a strong lithiophilicity to induce homogeneous distribution of the initial Li nucleus, further regulating subsequent Li growth [Figure 3C]. Moreover, the porous structure and excellent conductivity of the carbonaceous skeleton lowered the host current density effectively, further promoting the even deposition of Li. At 2 $mA·cm^{-2}$, the NGCF electrode can cycle 300 times, while planar Cu electrodes exhibited drastic fluctuations after a few cycles. Moreover, the overpotential of a symmetrical battery with a NGCF@Li electrode is only 15 mV; it can also maintain stably over 1,200 h.

Constructing high-performance Li anodes with other emerging technologies is feasible and efficient. Lyu *et al.* developed a N-doped carbon host (3DP-NC) [Figure 3D] via 3D-printing[80]. The 3DP-NC has N-doping carbon and large pores, which can alleviate the volume expansion and regulate Li metal. With the

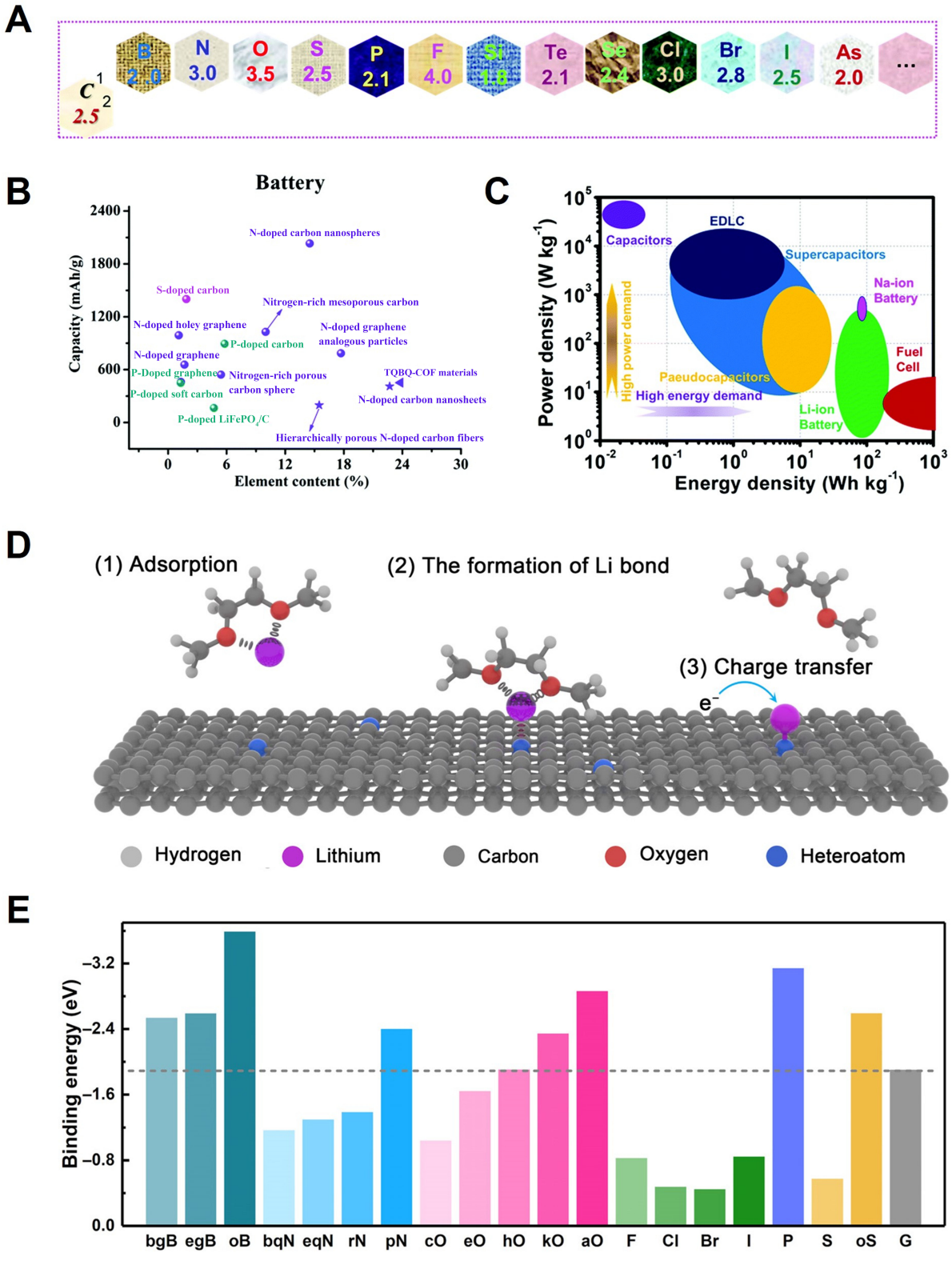

Figure 2. (A) Electronegativity values of various elements based on carbon; (B) The capacity of some reported heteroatom-doped carbon materials applied in batteries; (C) The energy density ranges of some common electrochemical energy storage devices. Reproduced with permission[73]. Copyright 2021, The Royal Society of Chemistry; (D) Li bond formation and nucleation process on the surface of carbon substrates; (E) The binding energy between Li atom and various elements. Reproduced with permission[75]. Copyright 2019, American Association for the Advancement of Science.

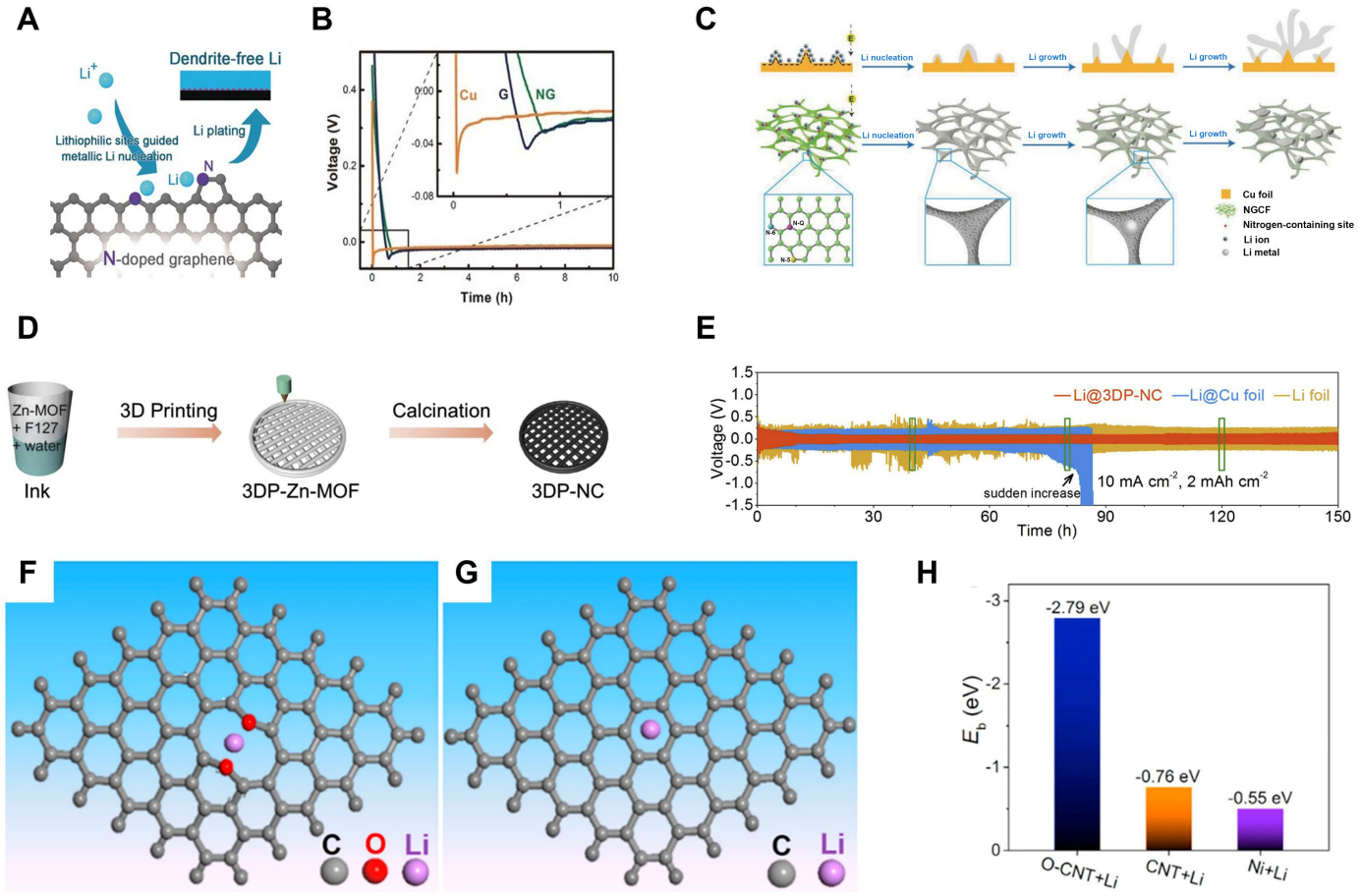

Figure 3. Composite Li anodes constructed by single heteroatom doping strategy. (A) The Li-N interaction guided dendrite-free Li plating; (B) Li nucleation voltage profile of Cu, G, and NG electrodes at 0.05 mA·cm^{-2}. Reproduced with permission[78]. Copyright 2017, Wiley-VCH; (C) The difference of Li deposition process on the bare Cu and NGCF electrodes. Reproduced with permission[79]. Copyright 2018, Wiley-VCH; (D) Preparation process of 3DP-NC electrode; (E) Galvanostatic cycling of three different electrodes at the current density of 10 mA·cm^{-2} with an area capacity of 2 mAh·cm^{-2}. Reproduced with permission[80]. Copyright 2020, Elsevier; (F) Optimized structure of the Li atom adsorbed on the C=O group containing graphene; (G) Optimized structure of the Li atom adsorbed on the pure graphene; (H) Adsorption energies of Li on O-CNT, CNT and Ni. Reproduced with permission[81]. Copyright 2018, Elsevier. NG: Graphene containing nitrogen; CNT: carbon nanotube.

test condition of 10 mA·cm^{-2} and 30 mAh·cm^{-2} [Figure 3E], the cell with this modified host still can deliver favorable performance. The 3D-printed technology sheds light on the quantity production of practical Li metal anodes.

Owing to the high electronegativity of oxygen (χ = 3.5), which leads to a strong interaction with Li atoms, the nucleation overpotential of Li is expected to be greatly reduced on the O-doped host. Liu *et al.* fabricated an O-doped carbon substrate [O-carbon nanotube (CNT)] as a 3D Li host via a "barbecue" approach[81]. The carbonyl (C=O) can interact strongly with Li atoms, guiding Li nucleate and grow homogeneously. Density functional theory (DFT) calculations verified the adsorption energies of O-CNT + Li are several times higher than CNT + Li and Ni + Li [Figure 3F-H]. Electrochemical tests also indicated that cells with O-CNT@Li electrodes have smaller voltage polarization and superior performance than CNT@Li and Ni foam (NF)@Li electrodes. This facile and scalable "barbecue" approach offers a novel approach for manufacturing the advanced Li batteries.

Codoping

Single heteroatom-doped hosts can adjust the Li deposition to some extent, but the regulation of the single element is limited. Codoped materials as Li hosts can further improve lithiophilicity via synergistic effects from different elements. N and P[82], N and O[83], N and S[84], and N and B[85] are the most widely adopted dual elements to fabricate heteroatom-doped materials. Carbon cloth, carbon paper (CP), Cu foil, *etc*. are employed to introduce heteroatoms in situ. With the influence of heteroatoms, the host surface exhibits a uniform Li^+ flux and subsequently forms dense Li deposition.

N, P codoped carbon cloth (NPCC) can be fabricated by simple polymerization and carbonization of carbon cloth [Figure 4A][82]. After carbonization, an interconnected carbon nanorod network parcelled the carbon fibers while pristine carbon cloth was smooth. Chemical composition detection confirmed the contents of N and P are around 2.1% and 1.0%, respectively, ensuring sufficient lithiophilicity of the carbon matrix. As a result, molten Li can be rapidly injected into the NPCC framework to form the NPCC-Li electrode. Symmetric cells assembled with NPCC-Li electrodes stably cycled over 600 h with a small voltage polarization of around 30 mV [Figure 4B]. What is more, the Li-iodine fuel cell with this electrode can retain 100% capacity over 4,000 cycles. This study indicates fabricating surface-modified 3D carbon frameworks for regulating Li deposition is highly efficient. The modified matrix is not limited to carbon cloth but also can be other carbon materials.

N, S are also favorable dual heteroatom-doped elements to construct a high-lithiophilic host. The electronic density and surface adsorption capacity of the host can be well regulated by codoping. For instance, Li *et al*. prepared a N and S codoped CP (NS-CP) via pyrolysis of polypyrrole and thiourea treated CP[84]. The NS-CP was further coated with a graphite film to obtain a graphite-based layer (GL)/NS-CP electrode [Figure 4C and D]. Theoretical calculations show that N, S-modified graphene is more lithiophilic than pristine graphene and other single-doped graphene, indicating the strong lithiophilicity of N, S codoped matrices. The synergistic effect from N and S greatly enhances the lithiophilicity of the skeleton so molten Li infuses into it easily. The Li-GL/NS-CP anode shows superior electrochemical performance compared with the pure Li anode and Li-NS-CP anode, including smaller overpotential, greater cyclic stability, and alleviative volume expansion [Figure 4E].

As shown in Figure 4F and G, an upright carbon host containing N and O [N, O-codoped vertical carbon nanosheet arrays on Cu foil (NOCA@Cu)] were demonstrated[83]. They found the orientation mode of polymer films of the Cu matrix would affect doping results and topological morphologies of carbon network. Meanwhile, the polymer is simply scraped on the surface of Cu foil (C@Cu) and treated in a thermal atmosphere. Both reserve polymer precursor morphology after pyrolysis, whereas the deposition morphologies of Li and battery performance are quite different. The CE of NOCA@Cu host can realize 98% CE after a cycle time of 1,300 h. However, C@Cu only sustains 350 h with a lower CE of 94.5%. Additionally, Li deposition on NOCA@Cu is confined inside the vertical channels of carbon nanosheet arrays and presents dendrite-free morphology due to the stark difference in the content of nitrogen species. The high content of pyrrolic (63.38%) and pyridinic nitrogen (22.03%) of the NOCA@Cu electrode ensures sufficient lithiophilicity of the substrate, which realizes dendrite-free Li deposition.

Among these highly electronegative elements, the dual-doping of O and boron (B), in particular, shows stronger lithiophilicity because of their larger dipole[75]. Based on this understanding, Xie *et al*. demonstrated B and O bi-functionalized carbon current collectors (OBHcCs) to stable Li metal deposition[85]. The heterogeneous nucleation of Li atoms on bare Cu leads to SEI fracture, resulting in heterogeneous Li^+ flux, and then Li metal deposits at the crack of SEI preferentially [Figure 4H]. In contrast, the uniform

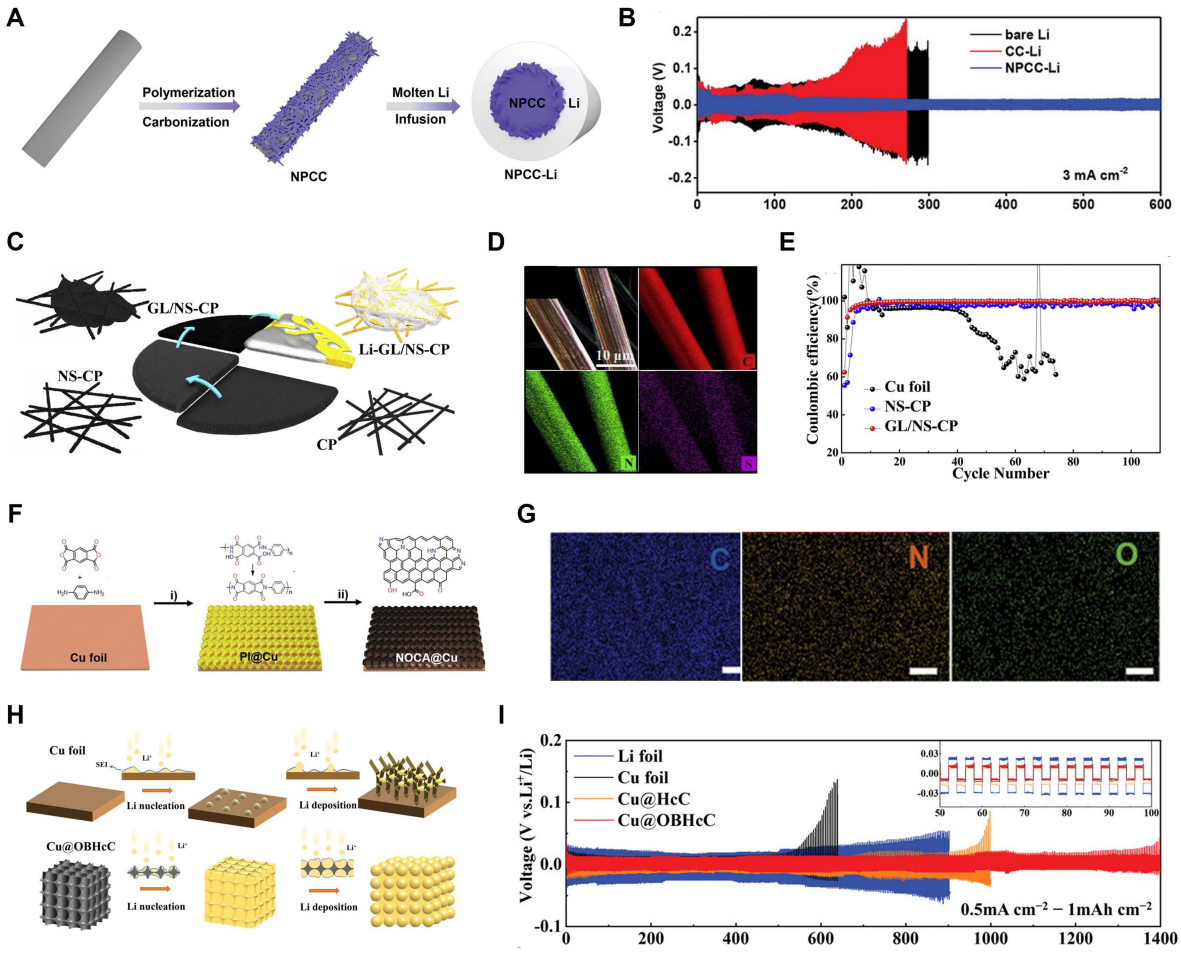

Figure 4. Composite Li anodes constructed by codoping strategy. (A) Scheme diagram of the synthetic procedure of NPCC-Li electrode; (B) Cycling stability of symmetric cells with different electrodes. Reproduced with permission[82]. Copyright 2019, Wiley-VCH; (C) Illustration of the preparation process of Li-GL/NS-CP electrode; (D) EDX mapping images of NS-CP. (E) CE test of Cu foil, NS-CP and GL/NS-CP electrodes at 1.0 mA·cm^{-2}. Reproduced with permission[84]. Copyright 2020, Elsevier; (F) Preparation process of hierarchical polymer/C sheet arrays on Cu electrode; (G) EDX mapping images of NOCA@Cu electrode. Reproduced with permission[83]. Copyright 2021, Wiley-VCH; (H) Li deposition behavior on the Cu substrate and Cu@OBHcC substrate; (I) Cycling stability of symmetric cells with different electrodes at a current density of 0.5 mA·cm^{-2}. Reproduced with permission[85]. Copyright 2022, Wiley-VCH. NPCC: N, P codoped carbon cloth; EDX: energy dispersive X-ray spectroscopy.

distribution of O/B doping sites on the honeycomb carbon skeleton greatly reduces the Li nucleation overpotential. Li metal can deposit uniformly along the honeycomb carbon skeleton on Cu@OBHcC current collectors and form a dense Li layer. In addition, the carbon skeleton with rich pores can effectively decrease the electrode current density to inhibit dendrite formation. The symmetric cells with Cu@OBHcC current collector maintained a stable voltage profile over 1,400 h [Figure 4I].

Different types of heteroatoms have their characteristics, so a reasonable configuration is needed to maximize their advantages. N or O atoms have strong electronegativity that can serve as active sites to interact with Li atoms, while doping of S or P can enlarge the layer distance of matrix materials, which facilitates the transport ability of Li^+. Despite the feasibility of codoping for constructing a composite Li anode with the above-mentioned atoms, we should recognize its deficiencies and challenges. According to electronegativities of elements reflected from the periodic table, many possible codoping combinations

exist, but only a few have been reported, indicating a wide gap between theoretical prediction and practical situations. Some previous works display satisfying electrochemical test results, but calculation modeling of doping lacks a unified standard and its internal mechanism remains indefinable. Even though doping is doable, accurately controlling the doping amounts and sites to further enhance the lithiophilicity of the host is also knotty. Most importantly, whether the selected doping strategy can achieve large-scale preparation and application needs to be considered. Therefore, further study of heteroatom-doped frameworks applied to Li metal anodes is necessary.

Doped hosts anchored with metal atoms

The introduction of highly electronegative heteroatoms into the carbon ring improves the host lithiophilicity. Since empty orbitals in metal atoms can interact with lone electron pairs of heteroatoms, we can further bring metal atoms into the doped carbon ring to form an M-N_x-C structure that contains carbon, nitrogen and metal sites simultaneously. Due to the presence of metal sites and nitrogen, the local electric field is regulated well, so the lithiophilic framework realizes dendrite-free morphology. Interestingly, researchers noted that some M-N_x-C structures can exert satisfactory lithiophilicity while maintaining structural stability[86]. This will be discussed in the next sections. Ni[87], Co[88], Mn[86], *etc*. are the widely used atoms to fabricate M-N doped structures.

Liu *et al*. reported an integrated lithiophilic framework with the Co atoms anchored in the N-doped carbon structure (CoNC)[88]. Different from the general metal particles-modified skeleton, the mixture of cobalt sources, carbon sources, and nitrogen sources can directly transform into N-doped carbon materials with Co-N_x-C moieties via simple carbonization treatment. Such atomically dispersed lithiophilic CoN_x Sites induce an enhanced electron cloud density so it can guide Li deposition effectively. Besides, the well-defined Co-N_x-C structure shows good wettability for electrolytes, which provides ceaseless Li^+ flux to achieve dense Li morphology. According to Figure 5A, the adsorption of Li atoms at a specific position shows a strong binding energy. However, it is only -0.86 eV of graphitic N-doped graphene (NG), indicating its weak adsorption capacity. Thus, the Li seed is random on the graphitic NG surface and gradually forms into Li clusters of diverse sizes. A Li deposition/stripping process with a CoNC@Li electrode displays a dendrite-free morphology. Moreover, CE using a CoNC electrode shows an ultrahigh value of 99.2% over 400 and 350 cycles at 2 and 5.0 mA·cm^{-2}, respectively, and even 98.2% at 10.0 mA·cm^{-2} [Figure 5B]. The $LiFePO_4$ (LFP) full cell using a CoNC@Li electrode also exhibits stable cycling ability. The strategy utilizing metal atoms-modified carbon substrate provides a new avenue for promoting Li metal anodes for practical application.

Although the above Co-N_x-C structure exhibited good lithiophilicity, the authors did not further evaluate the stability of the Co-N_x-C structure through experiments or theoretical calculations. Similar to Co atoms, Ni atoms also can form a Ni-N-C structure. Zhai *et al*. synthesized the Ni atom-modified graphene [single Ni atoms supported on NG (SANi-NG)][87]. Around the heteroatomic active sites, the SANi-NG shows moderate interaction strength toward Li, so it can maintain atomic structural stability simultaneously [Figure 5C]. DFT calculation results indicate that the lithiophilicity mechanism of SANi-NG is different from that of NG. Both possess appreciable Li adsorption energy, but the transformation of bond length is quite different after Li atoms are adsorbed. The more obvious change of the Li-N bond in NG damages its structure due to high-intensity bond interaction. The experimental results also verify the importance of the single-atom doping type for host structural stability.

A mainstream view is that the larger the binding energy, the better its ability to regulate Li deposition. Nevertheless, excessively strong interaction would trigger irreversible reactions thermodynamically, which

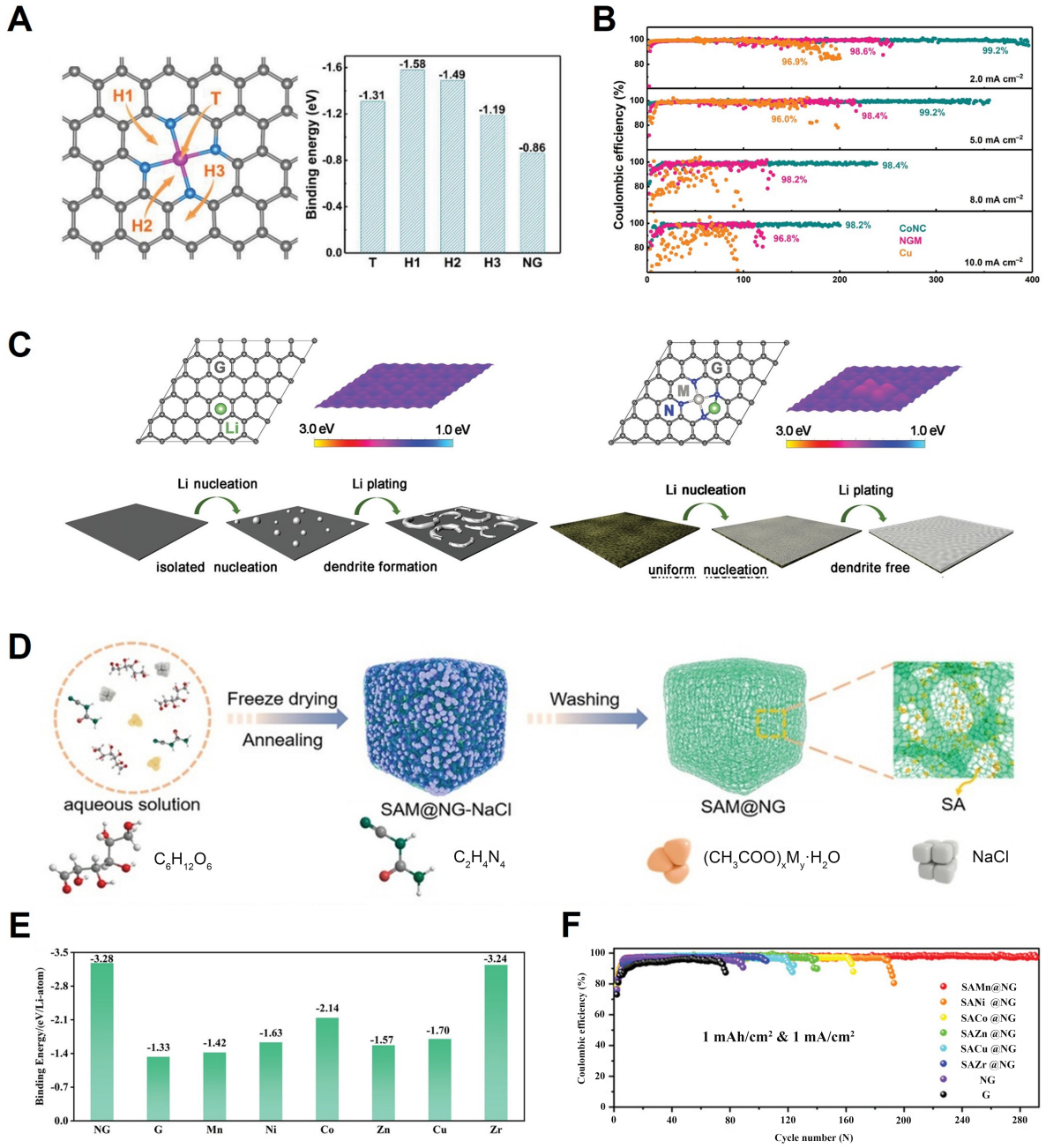

Figure 5. Composite Li anodes constructed by doped hosts anchored with metal atoms. (A) Structural model of CoNC on Li and binding energy of the corresponding sites; (B) CE test of CoNC, NGM, and Cu electrodes. Reproduced with permission[88]. Copyright 2018, Wiley-VCH; (C) The distribution of Li adsorption energy and Li nucleation/growth behavior on PG and SANi-NG electrodes. G is graphene, M is metal atom, N is nitrogen, and Li is Li atom, respectively. Reproduced with permission[87]. Copyright 2019, Wiley-VCH; (D) Schematic diagram of the SAM@NG synthesis; (E) Binding energy of Li atoms on different substrates; (F) CE test of different substrates with a capacity of 1 mAh·cm^{-2} at 1 mA·cm^{-2}. Reproduced with permission[86]. Copyright 2022, Wiley-VCH. CE: Coulombic efficiency; CoNC: Co atoms anchored in the N-doped carbon structure.

eventually results in the premature collapse of the lithiophilic sites. To confirm the above claims, Yang *et al.* further investigated several kinds of SAM@NG substrates [Figure 5D] (M = Ni, Co, Mn, Cu, Zn, Zr) based on the study of SANi-NG above and proposed the concept of reversible lithophilic sites[86]. They found the

binding energy between lithiophilic sites and Li atoms should not be too strong or too weak. Too strong interaction would lead to the structural damage, while a weak binding energy is not conducive to uniform Li nucleation. Only when binding energy is controlled in a certain range can the lithiophilicity be maximized. As shown in Figure 5E, the SAZr@NG and NG show binding energies of -3.24 and -3.28 eV, respectively. However, their electrochemical performances [Figure 5F] are much worse than SAMn@NG, whose binding energy to Li is -1.42 eV. Structural stability, analyzed via ab initio calculation, indicates that SAMn@NG shows the smallest bond transformation of Mn-Nx structure, which enables outstanding host stability after Li adsorption. We cannot just regard the binding energy as the sole criterion to evaluate the lithiophilic sites; we should also consider the change of bond length/bond angle before and after the adsorption of Li atoms. An idea lithiophilic sites should possess moderate binding energy and high structural stability.

Hosts modified with lithiophilic materials

In general, the pristine 3D current collector shows poor wettability for Li metal, which means a heterogeneous nucleation barrier to overcome. To give full play to the 3D skeleton, it is necessary to lower the energy barrier for Li on the skeleton surface and promote uniform nucleation. As described above, surface chemical properties and surface topography are important factors for wettability. So, reasonable designs are needed to change the properties of the substrate surface. Coating some functional materials on the host surface is an effective way to eliminate surface tension and accelerate Li infusion, further realizing uniform deposition and settling the interface instability triggered by the dendritic Li growth[89]. These functional materials include metallic oxides, metal nitrides (MNs), and metals that can form an alloying phase with Li. The electrochemical performance of these functional materials loading on a lithiophilic current collector is summarized in Table 2. Nucleation overpotential can be greatly decreased due to the stable interface layer generated from lithiation reaction with these metal compounds or solid solution formed by alloying reaction with metals. Moreover, the Li volume fluctuation is also solved well owing to the 3D structure of the substrate.

Metal-based oxides

In LIBs, metal-based oxides are widely used as electrode materials because they are inexpensive and have a high theoretical specific capacity. The oxygen in metal oxides exists as ions, so it exhibits strong adsorption toward the Li^+ near the anode. In this condition, the metal-based oxides (ZnO[90,91], CuO[92,93], Cu_2O[30], NiO[94,95], In_2O_3[96], *etc.*) can serve as seeds for selective Li metal deposition. Although most metal-based oxides would have a lithiation reaction with Li metal in the first cycle, uniform Li nucleation on the anode surface still can achieve profit from the highly dispersed lithiophilic seeds. As we know, the initial nucleation behavior is vital for subsequent Li metal deposition. The end products of lithiation reaction are generally metallic particles and Li_2O. Li_2O is a SEI component with good ionic conductivity, which can homogenize Li^+ and facilitate Li^+ transportation. So, the seeded growth pattern of Li at the first cycle and subsequent uniform Li deposition can be realized by coating metal-based oxides on the substrate.

Polyimide (PI) matrices possess prominent mechanical stability, heat-resisting properties, and chemical stability, which have potential as self-standing 3D Li hosts, but they show poor wettability for molten Li. For this reason, Liu *et al.* fabricated a modified PI matrix by coating a conformal layer of lithiophilic ZnO particles on its surface via atomic layer deposition[90] [Figure 6A]. Molten Li metal can infuse the core-shell PI-ZnO structure quickly and react with ZnO to form LiZn alloy and Li_2O. Both of the reaction products are favorable for interface stability. Most importantly, they found that Li plating/stripping within the Li-coated PI-ZnO electrode exhibits well-defined behavior. Li metal is preferentially deposited on the ZnO-coated PI fiber surface, and the Li metal on top fibers is dissolved preferentially in the first cycle. Therefore, the subsequent Li plating can be well-controlled by removing the conductive Li species. The exposed PI surface is electrically insulated, so Li preferentially deposits on the previously reserved Li surface instead of the

Table 2. A summary of electrochemical performance of lithiophilic-material loading host

Li Hosts	Materials	Li/Cu cells (current density; area capacity; cycle number; CE)	Symmetrical cells (current density; cycle time)	$LiFePO_4$ full cells (discharge current; cycle number; capacity retention)	Ref.
VA-CuO NSs	Vertically aligned CuO nanosheets	0.5 $mA·cm^{-2}$; 1 $mAh·cm^{-2}$; 180 cycles; 94% 1 $mA·cm^{-2}$; 1 $mAh·cm^{-2}$; 180 cycles; 94%	0.5 $mA·cm^{-2}$; 2 $mAh·cm^{-2}$; 700 h		[93]
CNT/NiO	Lotus-leaf-like 3D porous CNT/NiO		1 $mA·cm^{-2}$; 1 $mAh·cm^{-2}$; 600 h 3 $mA·cm^{-2}$; 1 $mAh·cm^{-2}$; 900 h	1 C; 300 cycles; 94.71%	[94]
BiOx/CC	BiOx-covered carbon cloth		1 $mA·cm^{-2}$; 1 $mAh·cm^{-2}$; 1,800 h 20 $mA·cm^{-2}$; 10 $mAh·cm^{-2}$; 250 h	1 C; 400 cycles; 84.4%	[97]
Co_3N/NF	Cobalt nitride nanobrush on a Ni foam	0.5 $mA·cm^{-2}$; 1 $mAh·cm^{-2}$; 200 cycles; 98.3% 1 $mA·cm^{-2}$; 1 $mAh·cm^{-2}$; 120 cycles; 96.9% 1 $mA·cm^{-2}$; 1 $mAh·cm^{-2}$; 150 cycles; 99.6%	0.5 $mA·cm^{-2}$; 1 $mAh·cm^{-2}$; 1,600 h 1 $mA·cm^{-2}$; 1 $mAh·cm^{-2}$; 1,200 h	0.5 C; 600 cycles; 93%	[100]
Mo_2N@CNF	Mo_2N-modified carbon nanofiber	4 $mA·cm^{-2}$; 3 $mAh·cm^{-2}$; 150 cycles; 99.2%	3 $mA·cm^{-2}$; 3 $mAh·cm^{-2}$; 1,500 h 6 $mA·cm^{-2}$; 6 $mAh·cm^{-2}$; 1,500 h		[102]
TiN-CNF	TiN-modified carbon nanofiber	1 $mA·cm^{-2}$; 1 $mAh·cm^{-2}$; 300 cycles; 95.8%	1 $mA·cm^{-2}$; 1 $mAh·cm^{-2}$; 600 h	1 C; 250 cycles	[104]
Carbon shell + Au NP		0.5 $mA·cm^{-2}$; 1 $mAh·cm^{-2}$; 300 cycles; 98%			[57]
LiSn	3D $Li/Li_{22}Sn_5$ nanocomposite foil		5 $mA·cm^{-2}$; 5 $mAh·cm^{-2}$; 400 h 10 $mA·cm^{-2}$; 5 $mAh·cm^{-2}$; 200 h 30 $mA·cm^{-2}$; 5 $mAh·cm^{-2}$; 67 h	5 C; 500 cycles; 91%	[116]
$Li_{20}Ag$		1 $mA·cm^{-2}$; 1 $mAh·cm^{-2}$; 400 cycles; 99.5%		1 C; 100 cycles; 92%	[108]
GaLi-Li			3 $mA·cm^{-2}$; 1 $mAh·cm^{-2}$; 800 h 5 $mA·cm^{-2}$; 1 $mAh·cm^{-2}$; 600 h 2 $mA·cm^{-2}$; 2 $mAh·cm^{-2}$; 300 h	2 C; 900 cycles	[117]

CE: Coulombic efficiency; VA-CuO NSs: vertically aligned CuO nanosheets; BiOx/CC: BiO_x-covered carbon cloth; Mo_2N@CNF: Mo_2N-modified carbon nanofiber; TiN-CNF: TiN-modified carbon nanofiber.

insulated PI surface. SEM characterization verifies the positive role for Li of PI-modified hosts. Nevertheless, excessive mossy Li can be observed at a low current density in the bare host. The rate performance of the Li-coacted PI-ZnO electrode exhibits significantly lower voltage hysteresis than the bare Li electrode under different current densities [Figure 6B]. Meanwhile, volume change caused by "host-less" behavior can be minimized due to Li storage within the PI matrix. Symmetric cells with Li-coacted PI-ZnO electrodes show flat voltage profiles and longer cycle stability than bare Li. This method, combining a non-conductive polymer matrix with lithiophilic particles to fabricate a structural Li anode, guides the rational design of Li hosts.

A thin CuO nanosheet [vertically aligned CuO nanosheets (VA-CuO NSs)] was formed in situ on a copper current collector and used as an advanced host[93]. As shown in Figure 6C, after immersing in an NH_4OH solution at 60 °C and drying, the Cu foil changes from golden to black, which indicates CuO nanosheets are successfully generated (VA-CuO-Cu). The molten Li spreads quickly and evenly on the modified current collector due to the lithiophilic nature of CuO while Li remains impermeable on the planar Cu [Figure 6D]. The surface morphology of pure Cu and modified electrodes after cycling are analyzed to understand clearly their distinct Li plating behavior. After 100 cycles, a lot of loose Li appears on the pure Cu. Some bulges cause uneven distribution of electric fields, forming so-called local hotspots and further aggravating the random growth of dendrites. In contrast, uniform and flat Li can be observed on VA-CuO-Cu hosts. Thanks to the smooth morphology, the full cell with a Li/VA-CuO-Cu electrode as an anode exhibits longer

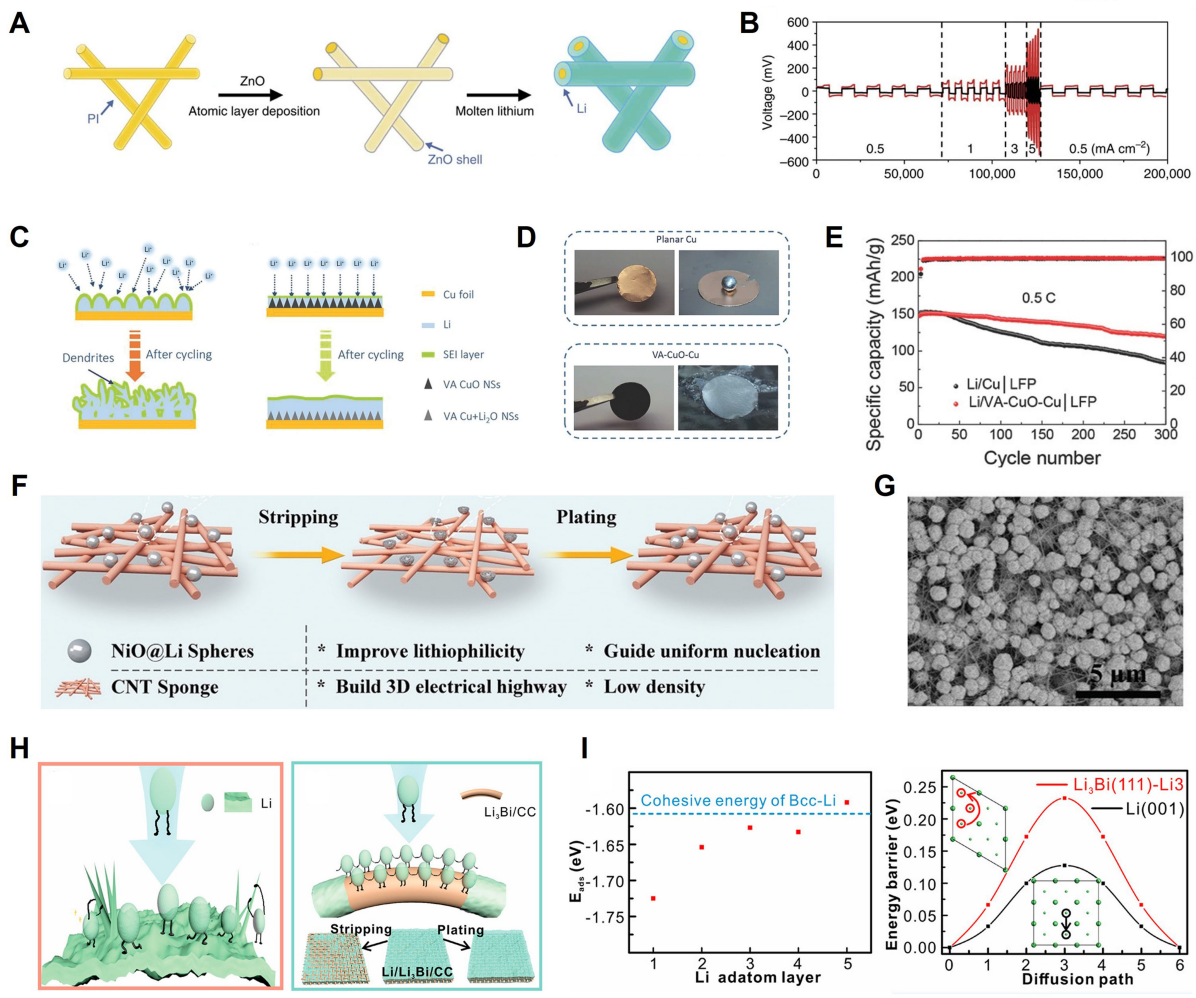

Figure 6. Composite Li anodes constructed with metal-based oxides. (A) Synthesis diagram of the Li-coated PI-ZnO electrode; (B) Rate test of Li-coated PI-ZnO electrode and pure Li electrode. Reproduced with permission[90]. Copyright 2016, Springer Nature; (C) Schematic diagram of Li deposition on bare Cu and VA-CuO-Cu electrode; (D) Molten Li diffusion on bare Cu electrode and VA-CuO-Cu electrode; (E) Cycle stability of Li/LFP full cells used pure Li and VA-CuO-Cu electrodes at 0.5 C. Reproduced with permission[93]. Copyright 2018, Wiley-VCH; (F) Schematic diagram of Li deposition/dissolution on bare Li electrode and CNT/NiO@Li electrode; (G) SEM image of the CNT/NiO substrate. Reproduced with permission[94]. Copyright 2021, Wiley-VCH; (H) Schematic diagram of Li plating and Li stripping on bare Li electrode and Li_3Bi/CC electrode; (I) The left figure is the cohesive energy of Li- Li_3Bi with different atom layers. Reproduced with permission[97]. Copyright 2021, American Chemical Society. LFP: $LiFePO_4$; CNT: carbon nanotube; CC: carbon cloth.

cycle life and higher capacity. The LFP-Li/VA-CuO-Cu full cell can maintain 97% capacity after 100 cycles while a LFP-Li/Cu cell is only 81.2% [Figure 6E]. Modifying the host through a simple chemical reaction is expected to find practical applications.

Using metal-based oxides as lithiophilic material to modify 3D current collectors has been widely recognized as an effective method, but the lithiophilicity mechanism is not fully understood. Although most oxides have been seen to undergo chemical reactions when cycling, we should give an insight into their other properties such as adsorption energy, diffusion barrier, surface topography, *etc*. Considering the molten Li and Li-active materials are liquid and solid, respectively, Mei *et al*. used the Wenzel model to explain the wettability of current collectors[94]. The Wenzel model is denoted as: $\cos\theta_w = r\cos\theta_1$, where θ_w is

the apparent contact angle; θ_1 is the intrinsic contact angle; r is the roughness factor. The apparent wetting behavior is related to the contact angle and the roughness of the substance surface. The higher wettability, the better the lithiophilicity, which can be achieved by introducing Li-active material on the matrix with a multiscale substructure. Hence, they constructed a 3D composite CNT/NiO host [Figure 6F] to enhance the wettability of Li metal, consisting of lithiophilic micro/nanostructured NiO particles and CNTs sponge [Figure 6G]. The highly conductive CNTs sponge accelerates charge transfer processes at the interface between CNTs and NiO particles. The anchored NiO particles with micro/nano size improve the lithiophilicity of hosts. Based on the optimized substrate and micro/nanostructure, the CNT/NiO-Li assembled symmetric cells can have a 900 h cycle life with a low 30 mV polarization. When cycled 300 times at 1C, the capacity of CNT/NiO-Li coupled LFP full cells can retain 94.71%, while the control full cells decay to 83.79%. The Wenzel wetting model provides significant guidance for constructing high wettability and lithiophilic host, revealing the Li wetting behavior from intrinsic contact angle and surface roughness.

Both adsorption energy and diffusion barriers are important for understanding the interaction between Li atoms and matrices, but the latter is rarely considered. The diffusion barrier is used to measure the difficulty level an adatom faces when migrating from one adsorption site to another. A low diffusion barrier facilitates the faster growth of Li clusters at new adsorption sites, which further evolves into Li dendrite. Therefore, constructing a lithiophilic framework with a moderate diffusion barrier is significant for dendrite-free Li plating. Xu *et al.* designed a BiO_x-covered carbon cloth (BiO_x/CC) to regulate uniform deposition through a thermodynamic aspect[97]. As shown in Figure 6H, the BiO_x changes into Li_3Bi in situ due to the reaction between BiO_x and Li. Theoretical calculations manifest that Li cohesive energy of Li_3Bi is larger than bulk Li, so Li deposits uniformly with the presence of Li_3Bi particles. Moreover, the adsorbed Li atoms on the Li_3Bi exhibit a high diffusion barrier [Figure 6I], preventing their migration to other fast-growing regions. With the suitable adsorption energy and diffusion barrier, Li dendrites are well inhibited. The Li_2O formed by melting Li can employed as a satisfactory SEI component to stabilize the interface. The Li_3Bi/CC-modified Li electrode enables the symmetrical cell to cycle over 250 h at high rates; a highly stable anode without dendrite Li will be achieved by designing lithiophilic substrates that can limit the free diffusion of Li atoms.

However, we need to note that metal-based oxides as lithiophilic materials also have many issues. Most metal-based oxides have poor electronic conductivity, which is bad for charge transfer between oxide and substrate[98]. The metal-based oxides based on chemical reaction will trigger volume change and inside stress to some extent when charging/discharging, which would result in lithiophilic particles detaching from the substrate. Some irreversible reactions between metal oxides and Li metal occur during discharge, which consumes part of the Li source and leads to low initial CE. In addition, we should consider the metal formed by the reaction of metal oxides with Li metal. Whether it has Li affinity significantly influences the interfacial durability.

Metal-based nitrides

MNs inherit the properties of transition metals but also give them some features of covalent compounds due to the nitrogen incorporation[99]. Unlike metal oxides, MNs show higher electronic conductivity and are expected to be candidate materials in the energy field. MNs (Co_3N[100], CoN[101], Mo_2N[102,103], TiN[104], Fe_3N[105], Cu_3N[106], *etc.*) also serve as ideal lithiophilic materials due to their excellent electronic conductivity and the intense tendency to form Li-N bonds. Due to various types of elements and crystal structures, these nitrides show different reactivity toward Li metal. Some nitrides have a conversion reaction with Li metal to form Li_3N while some others maintain high chemical stability during Li deposition/infusion. The latter can serve as homogeneous lithiophilic sites, accelerating charge transfer at the interface.

Lei *et al.* demonstrated a highly lithiophilic Co_3N coated Ni host (Co_3N/NF) via simple hydrothermal reaction and nitridation[100] [Figure 7A and B]. To highlight the superior lithiophilicity of Co_3N, they compared its electrochemical performance and Li deposition morphology with the CoO/NF counterpart. Owing to higher electronic conductivity than CoO, the Co_3N/NF shows lower interfacial impedance when cycling and reduces the generation of isolated Li. Moreover, both the CoO and Co_3N can undergo lithiation to form Li_2O and Li_3N, respectively, but Li_3N possesses higher Li^+ conductivity with a high Li^+ diffusion coefficient. Symmetrical cells with Li@Co_3N/NF composite anodes operate over 1,600 h. Besides, when Li plating/ stripping, the CE of Co_3N/NF can maintain at 98.3% over 200 cycles. All the electrochemical test results show that the Li@Co_3N/NF operates better than Li@CoO/NF electrodes. This work reveals the differences in lithiophilic behavior between metal oxides and nitrides. Both exhibit favorable affinity for Li and extend the lifespan of LMBs, but the nitrides have improved charge transfer dynamics and further reduced the interfacial impedance.

Mo_2N can also be converted into metallic Mo and Li_3N via lithiation reaction. Luo *et al.* demonstrated a Mo_2N-modified carbon nanofiber (Mo_2N@CNF) for uniform deposition, which enhances the Li affinity of carbon nanofibers (CNF) to a great extent[102]. X-ray photoelectron spectroscopy (XPS) characterization confirms the formation of the Mo and Li_3N phases after Li deposition [Figure 7C]. DFT calculation verified that the Li-Mo pairs display higher Crystal Orbital Hamilton Population (COHP) compared to Li-Li pairs, indicating that in-situ formed metallic Mo can serve as prior Li nucleation sites. Moreover, although Bader analysis shows that Li and Mo exhibit a bonding tendency, these two metals do not form intermetallic compounds under ambient conditions because of the insufficient driving power, thus avoiding the disorder of the interface [Figure 7D]. As shown in Figure 7E, the CE test displays the higher reversibility of Li plating/stripping on Mo_2N@CNF substrate than planar Cu and CNF. After 150 cycles, the Mo_2N@CNF substrate still can achieve an excellent CE of 99.6%. The symmetrical cells matched with Li-Mo_2N@CNF steadily cycle for more than 1,500 h. Most importantly, the capacity of full cells with Li-Mo_2N@CNF can maintain upon 90% when cycled 150 times.

Titanium nitride (TiN) not only exhibits great electronic conductivity and high chemical stability but also can induce the pseudocapacitive effect. The pseudocapacitive effect is favorable for highly reversible adsorption and desorption of Li^+ near anodes, which is further conducive to even Li plating/stripping under high current density. Based on this, Lin *et al.* presented a TiN-modified CNF (TiN-CNF) [Figure 7F] as a lithiophilic matrix to study the Li plating/stripping behavior[104]. Thanks to the lithiophilicity of TiN nanoparticles, Li is nucleated uniformly on the carbon fiber surface. The high electronic conductivity and rich pore structure of the carbon substrate also facilitate the charge transfer process and lower local current density. Theoretical calculations show that Li atoms have a low diffusion energy barrier on the TiN surface, further promoting Li deposition kinetics. Most importantly, the pseudocapacitive effect induced by TiN nanoparticles is confirmed by cyclic voltammetry (CV) measurement [Figure 7G]. Compared to the CNF electrode, the pseudocapacitive-dominated behavior of the TiN-CNF electrode contributes to faster kinetics, which is beneficial for the charge transfer process. When cycled over 200 times, the CE of TiN-CNF wrapped electrodes can reach 98.6%. In LFP full cells, the TiN-CNF composite anode with limited Li also delivers better cycling stability.

Alloys

The heterogeneous nucleation barrier needs to be overcome before forming Li seed on the substrates, which is manifested as the overpotential lower than mass transfer polarization. Although this overpotential exists in most substrates, Li can deliver an electrochemical alloying process with some metal substrates based on a solid-solution reaction to further reduce the nucleation barrier[107,108]. Metals such as Au[57,109,110], Ag[108,111,112],

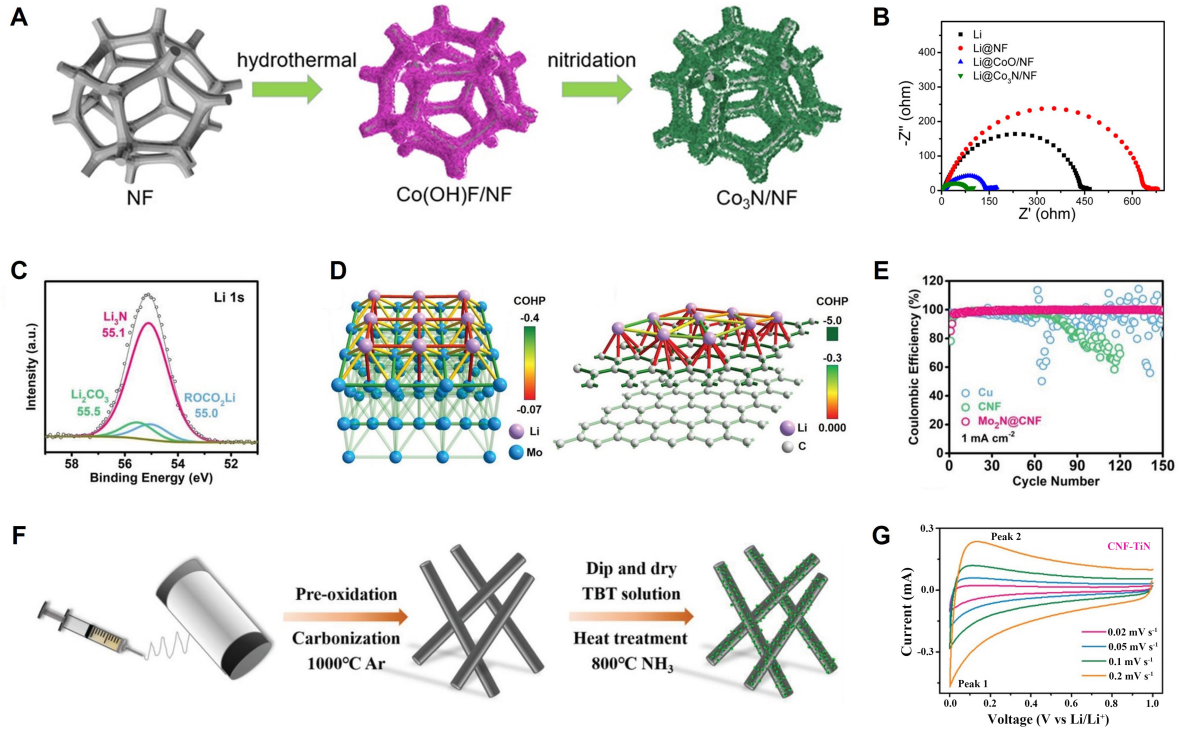

Figure 7. Composite Li anodes constructed by metal-based nitrides. (A) Schematic illustration of the preparation procedure of the Co_3N/NF electrode; (B) EIS spectra of bare Li, Li@NF, Li@CoO/NF, Li@Co_3N/NF electrode. Reproduced with permission[100]. Copyright 2019, American Chemical Society; (C) Li 1s XPS spectra of the lithiated Mo_2N@CNF electrode; (D) The calculation model of Li-Mo or Li-C clusters. The left figure is for the Li-Mo pairs and the right figure is for Li-C pairs; (E) CE test of different electrodes. Reproduced with permission[102]. Copyright 2019, Wiley-VCH; (F) Schematic diagram of the preparation procedure of the CNF-TiN electrode; (G) Cyclic voltammetry test of CNF-TiN electrode from 0.02 to 0.2 $mV \cdot s^{-1}$. Reproduced with permission[104]. Copyright 2019, Wiley-VCH. NF: Ni foam; XPS: X-ray photoelectron spectroscopy; CNF: carbon nanofiber.

Mg[113,114], Zn[113], Si[115], Sn[116], Ga[117], *etc.* can form an alloy phase with Li, which enhance the affinity between Li and the substrate. Nevertheless, we should note that some of them may cause significant volume fluctuation during the formation of alloys, which may interfere with the interface stability[118].

Yan *et al.* studied the Li nucleation behavior on Cu or Au matrices based on the Li-Cu and Li-Au phase diagrams[57]. When Li clusters formed on a Cu matrix, the large overpotential (40 mV) [Figure 8A] means an incompatibility between the two metals. On the contrary, the Li metal nucleation overpotential on lithiophilic Au is essentially zero. The nucleation condition of Li on the two substrates is correlated closely with their solubility. As shown in Figure 8B, Au and Li can form various forms of Li_xAu alloy in a wide range of Li atom ratios, with a solubility of 0.7% even when the ratio approaches 100%. This feature allows the Au metal to form Li-Au alloy in the full range and act as a buffer for smooth Li plating. However, there is no obvious alloying phase between Li and Cu. Based on the above discovery, they synthesized the Au nanoparticles-embedded hollow carbon nanoshells as hosts for Li deposition. Thanks to preferential Li nucleation at the location of Au "seeds", Li metal is successfully encapsulated inside the carbon nanoshells, which isolates the side reactions effectively. When cycled 300 times in carbonate electrolyte, the electrode (carbon shell + Au NP) through nano-encapsulation of Li can achieve an outstanding CE of 98%. Except for Au and Cu, the solubility of other metals toward Li and their effect on Li nucleation pattern has also been explored. It can be seen that a reasonably chosen metal substrate is crucial for ideal Li deposition.

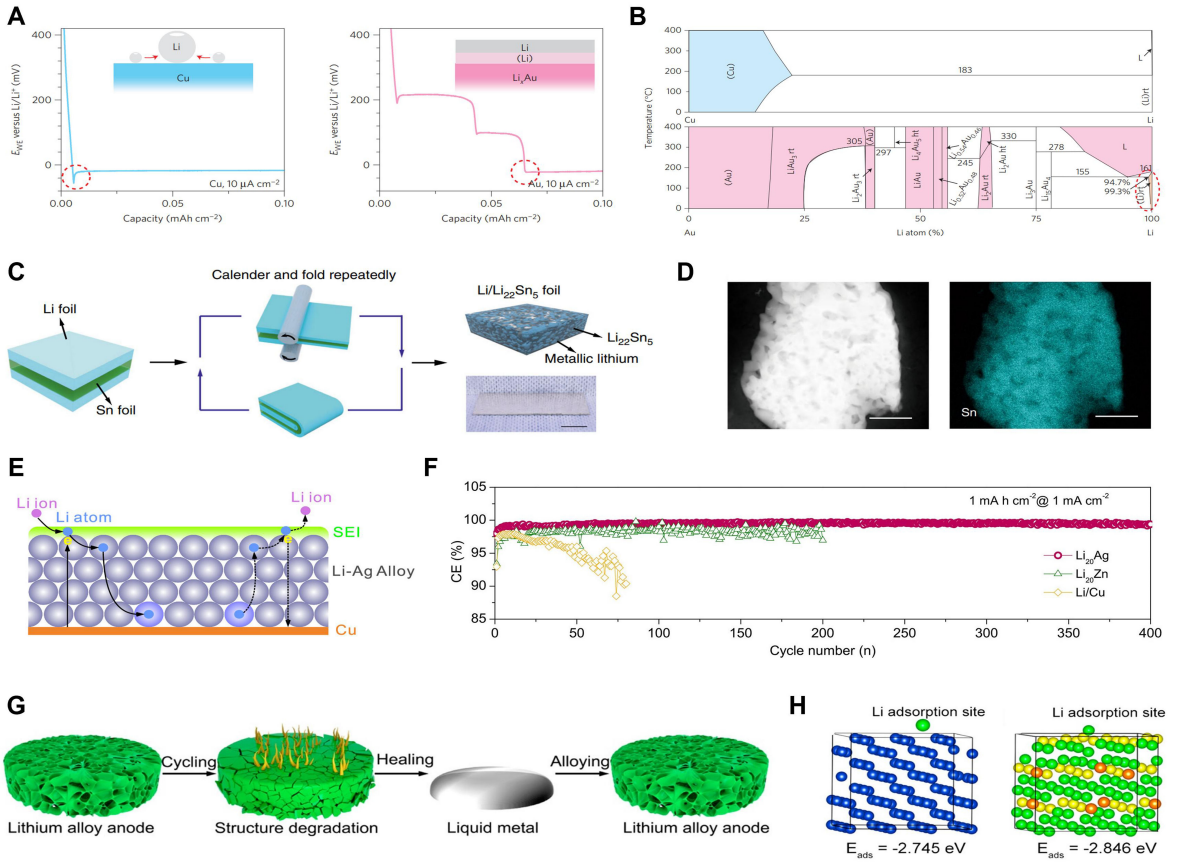

Figure 8. Composite Li anodes constructed by alloying strategy. (A) Li deposition curves on Cu substrate and Au substrate; (B) Binary metal phase diagrams of Li-Cu or Li-Au. Reproduced with permission[57]. Copyright 2016, Springer Nature; (C) Schematic diagram of the fabrication of the $Li/Li_{22}Sn_5$ foil; (D) TEM image of the $Li_{22}Sn_5$ electrode and the corresponding EDX mapping image of Sn element. Reproduced with permission[116]. Copyright 2020, Springer Nature; (E) Schematic diagram of alloying and dealloying of Li_xAg; (F) CE test of $Li_{20}Ag$, $Li_{20}Zn$, and Li/Cu electrodes at a current density of 1mA·cm^{-2} with an area capacity of 1mAh·cm^{-2}. Reproduced with permission[108]. Copyright 2020, American Chemical Society; (G) Schematic diagram of the electrode healing process of the HLAA; (H) Binding energy of Li-Cu (left) and Li-HLAA (right). Reproduced with permission[122]. Copyright 2021, American Chemical Society. TEM: Transmission electron microscopy; EDX: energy dispersive X-ray spectroscopy; HLAA: healable Li alloy anode.

Wan *et al.* demonstrated a three-dimensional (3D) and interpenetrated Li metal/LiSn alloy nanocomposite foil through simple calendering and folding[116] [Figure 8C and D]. The spontaneous alloying process reacts between the interface of Li and tin metal to obtain the 3D $Li/Li_{22}Sn_5$ structural anode. The $Li_{22}Sn_5$ displays the topology of interconnected frameworks with numerous interspaces after Li stripping from the initial composite anode [Figure 8D]. The 3D interconnected $Li_{22}Sn_5$ networks exhibit strong affinity and abundant interfaces for fast Li infusion and buffer volume change when battery charging/discharging. The unique nanostructure enables it to have a higher calculated contact area than the conventional Li composite anode, which prolongs the appearance of Sand's time. Interestingly, some unwanted by-products are intensified because the interface changes in a conventional Li/3D matrix, but they can be well suppressed in this interconnected structure. This is because the $Li_{22}Sn_5$ network can serve as a "pathway" for Li^+ transformation, and there is an essential discrepancy between $Li_{22}Sn_5$ and Li metal, so Li metal can deposit within the 3D network. Benefiting from the above, the $Li/Li_{22}Sn_5$ electrode functionalized symmetric cell shows low voltage polarization (~ 20 mV) at 200 cycles under 30 mAh·cm^{-2}. The corresponding full cells also hold a 91% initial capacity in 500 cycles at 5C.

Both Au and Sn can have alloying reactions with Li to form Li-Sn alloy phases, but they undergo different types of reactions. Au delivers a solid-solution reaction with Li, which helps to stabilize the interface, and the volume change is negligible[119,120]. The difference is that Sn would cause structure change during the lithiation-delithiation process due to its reconstitution reaction. Based on the solid solution reaction mechanism, Jin *et al.* demonstrate an inward-growth pattern of Li by utilizing the reversible alloying-dealloying reactions of Li on $Li_{20}Ag$ metal foil[108] [Figure 8E]. The newly reduced Li atoms can enter the $Li_{20}Ag$ metal foil during the alloying process and be dragged from inside when dealloying. The internal storage of Li atoms can reduce chaotic side reactions and avoid dendrite growth, which enables such composite Li anode to operate at lean electrolyte conditions. It should be noted that a $Li_{20}Zn$ electrode forms a LiZn intermetallic compound instead of a solid solution of Li and Zn. The different alloying behaviors of the two composite electrodes also lead to distinct electrochemical performance. Symmetric cells paired with $Li_{20}Ag$ electrodes stabilize over 2,000 h, while LiZn electrodes show short circuit phenomena at 480 h. The average CE value of $Li_{20}Zn$ electrodes is 98.2% in 200 cycles. In contrast, the Li_xAg electrode is 99.5% in 400 cycles with tiny fluctuation [Figure 8F]. The reversible solid-solution reaction can ensure the structural stability of the anode, which enables the fresh reduced Li atoms to infiltrate into the metal foil. This pattern of Li storage can achieve high-performance LMBs under limited electrolyte conditions.

Taking advantage of some special properties of liquid metals[121], Zhou *et al.* used gallium-indium to construct a healable Li alloy anode (HLAA), which can act as a highly lithiophilic metal matrix for Li regular deposition[122]. Impressively, this alloying electrode can renovate the degraded structure of hosts after Li extraction by turning into a liquid metal and become a composite anode again through the alloying reaction, which can keep the interface stability and framework integrity. As displayed in Figure 8G, although the HLAA degenerates after cycling caused by the parasitic side reaction and volume change, it still can revert to the eutectic state owing to the low melting points of Ga-In. The theoretical calculation indicates that HLAA has strong adsorption energy and a low Li migration barrier, promoting the mass transport of Li^+ [Figure 8H]. Because of this, Li metal achieves a nucleation overpotential of about 0 mV on HLAA electrodes. The HLAA exhibits great survivability when cycled over 1,300 times. Even under extreme test conditions, the HLAA electrode can still keep over 80 cycles. This novel alloy anode can hold a certain amount of Li, reducing volume change and avoiding dendrite formation. Meanwhile, its unique healable feature can ensure the integrity of electrode structure and its survivability.

Compared with pure Li metal, the alloying anode has a higher electrochemical potential, which means that its reaction activity is lower. Therefore, it is very promising to reduce the decomposition of the electrolyte on the anode side. The host structures modified with lithiophilic particles would cause severe Li loss due to its lithiation reaction with Li[91], while Li storage via alloying reaction has higher interfacial stability and less irreversibility. The composite anode, after dealloying, can continue to serve as a host to confine Li well. However, the volume change and electrode pulverization caused by the alloying/dealloying process will influence the electrode integrality[123]. The volume fluctuation can be alleviated to some extent by reducing the particle size of the alloy matrix or porous morphology to create some space between the particles, but the complex preparation process and the decreasing anode capacity need to be further considered.

Gradient skeleton

The 3D porous Li host can confine the Li metal within the skeleton well. Further configuration of the host by doping or modification can further enhance its lithiophilicty. However, the Li electrodeposition on the conductive matrix is a complex process related to the current density, the number of actual Li^+, and other factors. The anode near the separator is more available to receive Li^+ from the cathode. Moreover, the pores filled with electrolytes increase ionic resistance, which inhibits ions migration further into the skeleton. All these factors make Li^+ tend to be adsorbed on the top of the host and reduced, which is generally called the

"top-growth" pattern of Li metal[124]. Because Li cannot deposit within the skeleton, the lithiophilic sites lose their original function. What is more, this accelerates Li dendrites to aggregate on the upper area of the skeleton and increases the risk of short-circuiting. Therefore, it is particularly important to ensure the battery safety by regulating the deposition of Li metal through a reasonable host design based on spatial dimension.

Blindly using lithiophilic materials cannot prevent the dendrite growth at the interface well. The deposition interface must be shifted away from the anode/separator interface to accomplish the safety. Considering electrode structure, the top with low electronic conductivity and the bottom with high electronic conductivity would make the Li metal follow the "bottom growth" mode. Moreover, giving the bottom higher lithiophilicity can further induce preferential Li deposition in that region. Hence, constructing a Li host possessing gradient conductivity and lithiophilicity is an improved strategy to achieve selective Li deposition[125,126]. In addition, some mixed ion and electron-conducting skeletons brought about widespread attention because they also have effective improvement on Li plating/stripping in the entire scaffold[127]. The challenge is selecting low-barrier materials to construct uniform lithiophilic sites at the host bottom and evaluate the rationality of structure design. Generally, gradient structure can be divided into conductivity gradient (CG)[128,129], lithiophilicity gradient[130-132], and dual gradient skeleton[133,134]. Table 3 presents the progress of different lithiophilic hosts with the gradient skeleton strategy[124,128,130,131,135-139].

Conductivity gradient

The electric field on the anode surface influences the plating behavior of Li because Li^+ can only be reduced where they meet electrons. If the electric field increased successively from the separator to the current collector, it would conduce to guide bottom Li deposition in the current collector. Therefore, determining how to choose appropriate materials to design structures with gradient electronic conductivity is a concern of researchers.

As we know, highly conductive metal is favorable for charge transfer, and the Li^+ flux can be homogenized by the electronegative functional group of polymers. Combined with their respective advantages, Li *et al.* demonstrated a gradient conductive functionalized matrix [gradient conductive-dielectric framework (CDG-sponge)] by sputtering a thickness-dependent Ni film on a nonconducting polymer framework[128]. As shown in Figure 9A, the upper part of the host is melamine, with the thickness of the nickel layer intensifying downward, which constitutes a gradient conductive layer. With the regulation of an enhanced electric field at the bottom, Li deposits conformably follow a "bottom-deposition" manner and grow upward. Furthermore, the amine group of melamine can interact with Li^+ to decrease the concentration gradient. Compared to the completely conductive host or the completely non-conductive host, the CDG-sponge showed more stable cycle performance. Under 0.5 $mA{\cdot}cm^{-2}$, the CE of Li/Cu half cells used CDG-sponge in 500 cycles is 98.4%. Full cells assembled with Li@CDG-sponge electrode can also deliver 400 cycles. This method of obtaining Ni metal coating by magnetron sputtering is facile to achieve large-scale preparation and is compatible with industrial fabrication. Superior performance of Li anodes can be achieved when Ni is replaced with a more lithiophilic metal.

Hong *et al.* introduced an electronic CG host through a vacuum-assisted infiltration method as an effective measure to inhibit dendrite growth on the anode surface[135]. The CG consists of a top insulating layer of SiO_2 and CNFs, a middle layer of Cu nanowires (CuNWs) and CNFs with intermediate conductivity, and a bottom layer of CuNWs and CNFs [Figure 9B]. The moderate conductive properties of the intermediate layer can slow down the reaction rate and homogenize the Li^+ flux. COMSOL Multiphysics simulation also indicates Li^+ are more concentrated at the bottom of the CG system, which favors denser Li deposition.

Table 3. A summary of electrochemical performance of different lithiophilic hosts with gradient skeleton

Li Hosts	Materials	Li/Cu cells (current density; area capacity; cycle number; CE)	Symmetrical cells (current density; cycle time)	$LiFePO_4$ full cells (discharge current; cycle number; capacity retention)	Ref.
CDG	Conductive-dielectric gradient framework	0.5 $mA·cm^{-2}$; 1 $mAh·cm^{-2}$; 600 cycles; 97%	1 $mA·cm^{-2}$; 1 $mAh·cm^{-2}$; 780 h	1 C; 400 cycles; 87.6%	[128]
CG	Electronic conductivity gradient	0.5 $mA·cm^{-2}$; 1 $mAh·cm^{-2}$; 120 cycles; 96%	1 $mA·cm^{-2}$; 1 $mAh·cm^{-2}$; 500 h 5 $mA·cm^{-2}$; 1 $mAh·cm^{-2}$; 200 h		[135]
G-CNF	Gradient-distributed nucleation seeds on carbon nanofiber	0.5 $mA·cm^{-2}$; 700 cycles; 98.1%	0.2 $mA·cm^{-2}$; 0.2 $mAh·cm^{-2}$; 1,800 h	1 C; 300 cycles; 95.7%	[130]
CuSnAl@Cu			1 $mA·cm^{-2}$; 1 $mAh·cm^{-2}$; 2,000 h	1 C; 300 cycles; 62%	[131]
DRS	Deposition-regulating scaffold	1 $mA·cm^{-2}$; 1 $mAh·cm^{-2}$; 500 cycles; 98.1% 0.5 $mA·cm^{-2}$; 2 $mAh·cm^{-2}$; 350 cycles; 97.0%	2 $mA·cm^{-2}$; 3.5 $mAh·cm^{-2}$; 500 h 10 $mA·cm^{-2}$; 3.5 $mAh·cm^{-2}$; 120 h		[136]
IAG	Interfacial activity gradient		1 $mA·cm^{-2}$; 1 $mAh·cm^{-2}$; 240 h	1 C; 250 cycles	[137]
SiC/CC	SiC whiskers and carbon cloth	1 $mA·cm^{-2}$; 1 $mAh·cm^{-2}$; 100 cycles; 95.0%	1 $mA·cm^{-2}$; 1 $mAh·cm^{-2}$; 1,000 h 5 $mA·cm^{-2}$; 5 $mAh·cm^{-2}$; 325 h	0.5 C; 120 cycles; 80%	[124]
GPCS		0.5 $mA·cm^{-2}$; 1 $mAh·cm^{-2}$; 320 cycles; 98.0%	1 $mA·cm^{-2}$; 1 $mAh·cm^{-2}$; 1,000 h	0.7 C; 600 cycles; 99.9%	[138]
Ni_2P/Ni_3S_2 NWs-NF	Upper Ni_3S_2 nanowires and bottom Ni_2P nanowires	1 $mA·cm^{-2}$; 1 $mAh·cm^{-2}$; 250 cycles; 98.0% 3 $mA·cm^{-2}$; 1 $mAh·cm^{-2}$; 250 cycles; 98.4%	1 $mA·cm^{-2}$; 1 $mAh·cm^{-2}$; 800 h 10 $mA·cm^{-2}$; 5 $mAh·cm^{-2}$; 180 h	1 C; 500 cycles; 91.4%	[139]

CE: Coulombic efficiency; CDG: conductive-dielectric gradient; CG: conductivity gradient; G-CNF: gradient-type carbon fiber modified with lithiophilic seeds; DRS: deposition-regulating scaffold; IAG: interfacial activity gradient; CC: carbon cloth.

Compared to Cu foil and CuNWs, the CG hosts achieve a higher CE in the symmetric cells and longer cycle life in the full cell coupled with NCM-811 cathodes. This study shows that the composition and structure of the intermediate layer is significant for uniform Li^+ flux. In addition, high conductivity of the bottom layer is beneficial for low R_{ct} (resistance of charge transfer) which facilitates the deposition dynamics.

Lithiophilicity gradient

The Li^+ flux from the separator to the anode surface can be directly regulated by frameworks with lithiophilicity gradient. Some common lithiophilic materials, such as Ag, Au, ZnO, *etc.*, and lithiophobic materials, such as Ni, Cu, Al_2O_3, *etc.*, are used to construct the lithiophilicity gradient. Moreover, gradient-distributed structures can be obtained by adjusting the concentration and thickness of lithiophilic materials on the 3D frameworks.

A gradient-type carbon fiber modified with lithiophilic seeds (G-CNF) was proposed by Nan *et al.*[130]. Th Li morphology of the G-CNF host is quite from CNF and ZnO-CNF hosts [Figure 9C]. In the direction of inverse Li^+ concentration distribution, the ZnO particles with gradient structure facilitate Li deposition in a vertical direction, which avoids reproducing isolated Li at the host top. However, Li metal of the uniform ZnO-modified CNF host or pure CNF tends to exhibit "top-growth" behavior and form dendrites. Electrochemical performance tests show that half-cells assisted by G-CNF can operate over 1,400 h, which indicates the high reversibility of Li plating/stripping. SEM characterization of Li deposition confirms its dendrite-free feature with the G-CNF electrode. Countering Li^+ concentration polarization via conductive

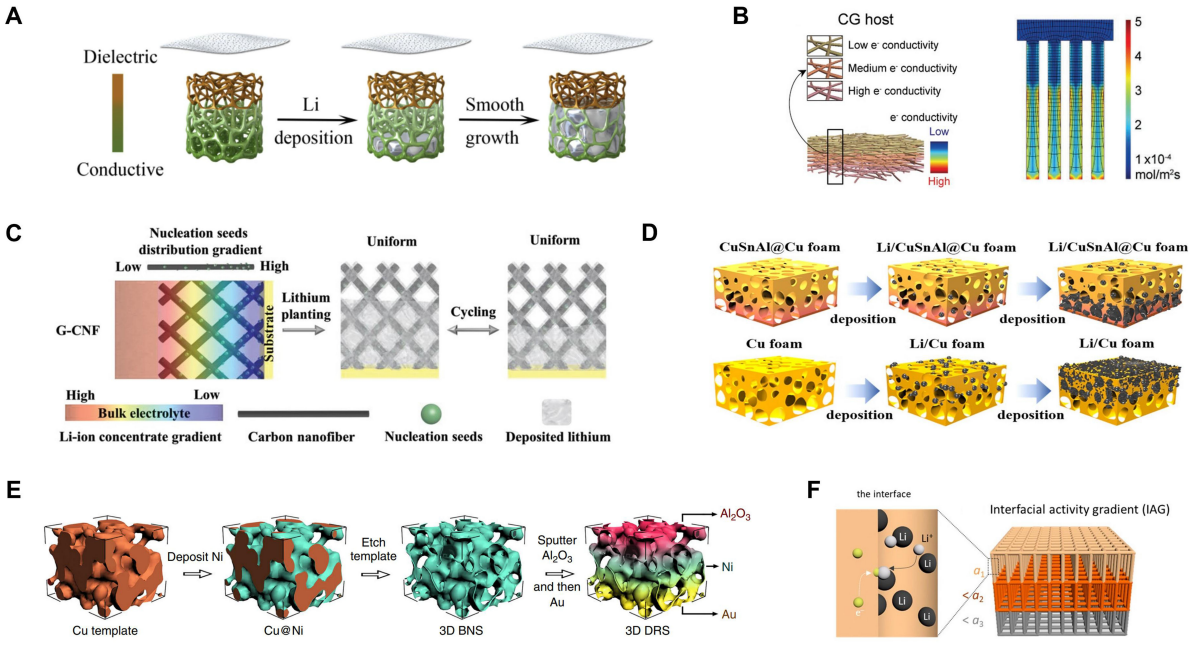

Figure 9. Composite Li anodes constructed by gradient skeleton. (A) Schematic diagram of "bottom-up" Li plating in CDG-sponge. Reproduced with permission[128]. Copyright 2020, Elsevier; (B) Schematic diagram of the CG host structure and Li-ion reaction flux modeled using COMSOL Multiphysics. Reproduced with permission[135]. Copyright 2020, Wiley-VCH; (C) Schematic of the G-CNF electrode in regulating Li deposition. Reproduced with permission[130]. Copyright 2019, Wiley-VCH; (D) Schematic of Li deposition behavior on CuSnAl@Cu electrode and pure Cu foam. Reproduced with permission[131]. Copyright 2022, American Chemical Society; (E) Preparation procedure of the DRS host. Reproduced with permission[136]. Copyright 2019, Springer Nature; (F) Schematic of the interfacial activity gradient. Reproduced with permission[137]. Copyright 2020, American Chemical Society. CDG: Conductive-dielectric gradient; CG: conductivity gradient; G-CNF: gradient-type carbon fiber modified with lithiophilic seeds.

hosts with gradient-distributed nucleation seeds can stabilize Li metal anodes to achieve "bottom-deposition" modes.

To reveal how the porous structure affects the Li deposition, Lv *et al.* sputtered a lithiophilic CuSnAl film on the Cu foam (CuSnAl@Cu) to remove the "top growth" of Li metal[131]. Li nucleation is preferentially at Sn sites due to the great lithiophilicity compared to pure Cu foam. The "bottom-up growth" mode of Li metal takes full advantage of the inner pores of the electrode [Figure 9D], which accommodates volume change and reduces the risk of short circuits. Experimental analysis confirms that the CuSnAl layer has lower electric potential, which reduces the Li^+ migration barrier in the bottom region. Benefiting from the lithiophilicity gradient structure, symmetrical cells with CuSnAl@Cu foam keep a steady cycling over 2,000 h. Furthermore, The CE of the LFP full cells assembled with CuSnAl@Cu-modified anodes can achieve 99.6% after 300 cycles.

Dual gradient structure

A *single* conductive or lithiophilic gradient is limited for regulating Li metal deposition. Construction of a dual gradient structure with both excellent conductivity and lithiophilicity can promote the deposition kinetics of Li^+ and electrons. Pu *et al.* reported a deposition-regulating scaffold (DRS) via electrodeposition, template etching, and sputtering[136]. As shown in Figure 9E, the 3D scaffold is made of Al_2O_3 at the top, Ni in the middle, and Au at the bottom. Interestingly, the transition among the three different parts can be connected well using a sputtering method. Al_2O_3 was chosen because of its electric passivation properties compared to the metallic Ni and Au, which avoid Li metal deposition at the top. In addition, the bottom Au

is super lithiophilicity compared to high barrier Al_2O_3, which is a preferred deposition site for Li metal. Under the dual regulation of conductive and lithiophilic gradients, the Li can be restricted well in the bottom of the host and highly reversible. The CE of DRS electrodes is 98.1% after 500 cycles. However, the CE of bare nickel scaffolds (BNS) with no gradient structure decreases rapidly after 80 cycles. The possibility of short circuits caused by Li dendrites is greatly reduced owing to the DRS with a bottom-deposition mode. Moreover, this metallic scaffold has high mechanical strength and large interior space, which can accommodate intense volume expansion.

According to the Li reaction kinetics, Yun *et al.* presented an interfacial activity gradient (IAG) to solve "top-growth" issues[137]. The 3D Cu mesh host is tailored with passivated polyvinylidene fluoride (PVDF) at the top and activated Ag at the bottom [Figure 9F]. Ag exhibits a strong affinity for Li, allowing uniform Li nucleation and growth. AC-impedance spectroscopy indicates the Cu surface with Ag and PVDF showed increased and decreased exchange current density, respectively, which verified the successful construction of IAG. Thanks to the IAG structure, the electrode exhibits reversible Li plating/stripping, and the cycle stability is more than two times compared to the control Cu electrode.

CONCLUSION AND OUTLOOK

The high activity and biased one-dimensional deposition characteristic of Li^0 lead to various irreversible reactions in the working process of LMBs, increasing the risk of dendrite formation. In addition, the volume of Li varies noticeably during the cycling. These challenges significantly impede its development. Some studies have used composite structured anodes to eliminate the volume expansion phenomenon during battery operation. Regrettably, due to the pore-rich structure and large thickness of these 3D Li hosts, on the one hand, it increases the probability of side reactions. On the other hand, it also intensifies the Li^+ concentration polarization inside the battery, making it impossible for Li^+ to completely and uniformly deposit inside the host. In recent years, it has been found that by imbuing the host with Li affinity, the early stages of Li deposition can be thermodynamically adjusted, ensuring uniform Li nucleation and growth, and achieving some progress. However, it also should be noted that several puzzlements remain to be clarified and handled in the lithiophilic host. Firstly, what exactly is lithiophilicity? One of the fundamental properties of lithiophilicity that has been accepted is the overpotential reduction during the nucleation stage of Li metal. More crucially, several studies indicate that another feature of lithiophilicity is that lithiophilic materials frequently have good compatibility or high binding energy with Li metal (Li^0). Additionally, a number of studies have shown that some polymer materials containing polar groups also have an attraction for Li^+, which affects the diffusion and transport pathways of Li^+, also known as lithiophilicity[140-142]. Thus, it is unclear whether the lithiophilicity is for Li^+ or Li atoms. Secondly, the intrinsic quality of lithiophilicity and its failure mechanism need further analysis[25]. In summary, some lithiophilic materials exert their lithiophilicity through alloying reactions, chemical/physical adsorption of Li, or redox reactions. As a result of these reactions, some lithiophilic sites undergo irreversible chemical reactions and are covered with "dead Li", making these lithiophilic sites unable to play their expected roles. Therefore, a thorough analysis for the interaction principles of these lithiophilic materials and the failure causes of lithiophilic sites can help us to design more stable lithiophilic hosts, ensuring the security and stability of Li batteries.

Overall, these lithiophilic hosts have shown promise in developing high-performance Li anodes. Even so, further study on the intrinsic properties of Li metal anodes is required, implying that future researchers should focus on thermodynamics, dynamics, micromechanics, and other factors. We expect that additional novel theories and design strategies on lithiophilicity will emerge in future and that LMBs will evolve and mature quickly so that we can enjoy the convenience they provide to our lives.

DECLARATIONS

Authors' contributions

Wrote the manuscript: Huang L, Li W
Discussed and reviewed the manuscript: Huang L, Li W, Cui Z

Availability of data and materials

Not applicable.

Financial support and sponsorship

This work was supported by the National Natural Science Foundation of China (Project No. 22072048) and the Guangdong Provincial Department of Science and Technology (Project No. 2021A1515010128 and No. 2022A0505050013)

Conflicts of interest

All authors declared that there are no conflicts of interest.

Ethical approval and consent to participate

Not applicable.

Consent for publication

Not applicable.

REFERENCES

1. Zhang JG, Xu W, Xiao J, Cao X, Liu J. Lithium metal anodes with nonaqueous electrolytes. *Chem Rev* 2020;120:13312-48. DOI PubMed
2. Zhou F, Xin S, Liang HW, Song LT, Yu SH. Carbon nanofibers decorated with molybdenum disulfide nanosheets: synergistic lithium storage and enhanced electrochemical performance. *Angew Chem Int Ed Engl* 2014;53:11552-6. DOI PubMed
3. Chen H, Yang Y, Boyle DT, et al. Free-standing ultrathin lithium metal-graphene oxide host foils with controllable thickness for lithium batteries. *Nat Energy* 2021;6:790-8. DOI
4. Wu F, Maier J, Yu Y. Guidelines and trends for next-generation rechargeable lithium and lithium-ion batteries. *Chem Soc Rev* 2020;49:1569-614. DOI PubMed
5. Cheng XB, Zhang R, Zhao CZ, Zhang Q. Toward safe lithium metal anode in rechargeable batteries: a review. *Chem Rev* 2017;117:10403-73. DOI PubMed
6. Zeng X, Li M, Abd El-hady D, et al. Commercialization of lithium battery technologies for electric vehicles. *Adv Energy Mater* 2019;9:1900161. DOI
7. Harper G, Sommerville R, Kendrick E, et al. Recycling lithium-ion batteries from electric vehicles. *Nature* 2019;575:75-86. DOI PubMed
8. Manthiram A. A reflection on lithium-ion battery cathode chemistry. *Nat Commun* 2020;11:1550. DOI PubMed PMC
9. Zhu P, Gastol D, Marshall J, Sommerville R, Goodship V, Kendrick E. A review of current collectors for lithium-ion batteries. *J Power Sources* 2021;485:229321. DOI
10. Gupta A, Manthiram A. Designing advanced lithium-based batteries for low-temperature conditions. *Adv Energy Mater* 2020;10:2001972. DOI PubMed PMC
11. Albertus P, Babinec S, Litzelman S, Newman A. Status and challenges in enabling the lithium metal electrode for high-energy and low-cost rechargeable batteries. *Nat Energy* 2018;3:16-21. DOI
12. Duffner F, Kronemeyer N, Tübke J, Leker J, Winter M, Schmuch R. Post-lithium-ion battery cell production and its compatibility with lithium-ion cell production infrastructure. *Nat Energy* 2021;6:123-34. DOI
13. Frith JT, Lacey MJ, Ulissi U. A non-academic perspective on the future of lithium-based batteries. *Nat Commun* 2023;14:420. DOI PubMed PMC
14. Tikekar MD, Choudhury S, Tu Z, Archer LA. Design principles for electrolytes and interfaces for stable lithium-metal batteries. *Nat Energy* 2016;1:16144. DOI

15. Ghazi ZA, Sun Z, Sun C, et al. Key aspects of lithium metal anodes for lithium metal batteries. *Small* 2019;15:e1900687. DOI PubMed
16. Wang Q, Liu B, Shen Y, et al. Confronting the challenges in lithium anodes for lithium metal batteries. *Adv Sci* 2021;8:e2101111. DOI PubMed PMC
17. Lin L, Qin K, Hu YS, et al. A better choice to achieve high volumetric energy density: anode-free lithium-metal batteries. *Adv Mater* 2022;34:e2110323. DOI PubMed
18. Wang T, Liu X, Zhao X, He P, Nan C, Fan L. Regulating uniform Li plating/stripping via dual-conductive metal-organic frameworks for high-rate lithium metal batteries. *Adv Funct Mater* 2020;30:2000786. DOI
19. Wang H, Xu Q. Materials Design for rechargeable metal-air batteries. *Matter* 2019;1:565-95. DOI
20. Lai J, Xing Y, Chen N, Li L, Wu F, Chen R. Electrolytes for rechargeable lithium-air batteries. *Angew Chem Int Ed Engl* 2020;59:2974-97. DOI PubMed
21. Liu T, Vivek JP, Zhao EW, Lei J, Garcia-Araez N, Grey CP. Current challenges and routes forward for nonaqueous lithium-air batteries. *Chem Rev* 2020;120:6558-625. DOI PubMed
22. Bruce PG, Freunberger SA, Hardwick LJ, Tarascon JM. Li-O_2 and Li-S batteries with high energy storage. *Nat Mater* 2011;11:19-29. DOI PubMed
23. Gao Y, Guo Q, Zhang Q, Cui Y, Zheng Z. Fibrous materials for flexible Li-S battery. *Adv Energy Mater* 2021;11:2002580. DOI
24. Shen X, Liu H, Cheng X, Yan C, Huang J. Beyond lithium ion batteries: higher energy density battery systems based on lithium metal anodes. *Energy Storage Mater* 2018;12:161-75. DOI
25. Zhan Y, Shi P, Ma X, et al. Failure mechanism of lithiophilic sites in composite lithium metal anode under practical conditions. *Adv Energy Mater* 2022;12:2103291. DOI
26. Yuan H, Ding X, Liu T, et al. A review of concepts and contributions in lithium metal anode development. *Mater Today* 2022;53:173-96. DOI
27. Yang CP, Yin YX, Zhang SF, Li NW, Guo YG. Accommodating lithium into 3D current collectors with a submicron skeleton towards long-life lithium metal anodes. *Nat Commun* 2015;6:8058. DOI PubMed PMC
28. Mao H, Yu W, Cai Z, et al. Current-density regulating lithium metal directional deposition for long cycle-life Li metal batteries. *Angew Chem Int Ed Engl* 2021;60:19306-13. DOI PubMed
29. Ye Y, Zhao Y, Zhao T, et al. An antipulverization and high-continuity lithium metal anode for high-energy lithium batteries. *Adv Mater* 2021;33:e2105029. DOI
30. Liu Y, Zhang S, Qin X, Kang F, Chen G, Li B. In-plane highly dispersed Cu_2O nanoparticles for seeded lithium deposition. *Nano Lett* 2019;19:4601-7. DOI PubMed
31. Ma Y, Wei L, He Y, et al. A "blockchain" synergy in conductive polymer-filled metal-organic frameworks for dendrite-free li plating/stripping with high coulombic efficiency. *Angew Chem Int Ed Engl* 2022;61:e202116291. DOI PubMed
32. Lin D, Liu Y, Liang Z, et al. Layered reduced graphene oxide with nanoscale interlayer gaps as a stable host for lithium metal anodes. *Nat Nanotechnol* 2016;11:626-32. DOI PubMed
33. Cai Q, Qin X, Lin K, et al. Gradient structure design of a floatable host for preferential lithium deposition. *Nano Lett* 2021;21:10252-9. DOI PubMed
34. Hu Z, Su H, Zhou M, et al. Lithiophilic carbon nanofiber/graphene nanosheet composite scaffold prepared by a scalable and controllable biofabrication method for ultrastable dendrite-free lithium-metal anodes. *Small* 2022;18:e2104735. DOI PubMed
35. Liu F, Xu R, Wu Y, et al. Dynamic spatial progression of isolated lithium during battery operations. *Nature* 2021;600:659-63. DOI PubMed
36. Piao Z, Gao R, Liu Y, Zhou G, Cheng HM. A review on regulating Li^+ solvation structures in carbonate electrolytes for lithium metal batteries. *Adv Mater* 2023;35:e2206009. DOI PubMed
37. Jin C, Liu T, Sheng O, et al. Rejuvenating dead lithium supply in lithium metal anodes by iodine redox. *Nat Energy* 2021;6:378-87. DOI
38. Jiang Z, Zeng Z, Liang X, et al. Fluorobenzene, a low-density, economical, and bifunctional hydrocarbon cosolvent for practical lithium metal batteries. *Adv Funct Mater* 2021;31:2005991. DOI
39. Lee SH, Hwang J, Ming J, et al. Toward the sustainable lithium metal batteries with a new electrolyte solvation chemistry. *Adv Energy Mater* 2020;10:2000567. DOI
40. Reinoso DM, Frechero MA. Strategies for rational design of polymer-based solid electrolytes for advanced lithium energy storage applications. *Energy Storage Mater* 2022;52:430-64. DOI
41. Zhang J, Zeng Y, Li Q, et al. Polymer-in-salt electrolyte enables ultrahigh ionic conductivity for advanced solid-state lithium metal batteries. *Energy Storage Mater* 2023;54:440-9. DOI
42. Xu L, Lu Y, Zhao C, et al. Toward the scale-up of solid-state lithium metal batteries: the gaps between lab-level cells and practical large-format batteries. *Adv Energy Mater* 2021;11:2002360. DOI
43. Famprikis T, Canepa P, Dawson JA, Islam MS, Masquelier C. Fundamentals of inorganic solid-state electrolytes for batteries. *Nat Mater* 2019;18:1278-91. DOI PubMed
44. Yu Z, Cui Y, Bao Z. Design principles of artificial solid electrolyte interphases for lithium-metal anodes. *Cell Rep Phys Sci* 2020;1:100119. DOI
45. Gao RM, Yang H, Wang CY, Ye H, Cao FF, Guo ZP. Fatigue-resistant interfacial layer for safe lithium metal batteries. *Angew Chem*

Int Ed Engl 2021;60:25508-13. DOI PubMed
46. Sun Y, Zhao Y, Wang J, et al. A novel organic "polyurea" thin film for ultralong-life lithium-metal anodes via molecular-layer deposition. *Adv Mater* 2019;31:e1806541. DOI PubMed
47. Yang C, Yao Y, He S, Xie H, Hitz E, Hu L. Ultrafine silver nanoparticles for seeded lithium deposition toward stable lithium metal anode. *Adv Mater* 2017:29. DOI PubMed
48. Dong K, Xu Y, Tan J, et al. Unravelling the mechanism of lithium nucleation and growth and the interaction with the solid electrolyte interface. *ACS Energy Lett* 2021;6:1719-28. DOI
49. Hou LP, Yao N, Xie J, et al. Modification of nitrate ion enables stable solid electrolyte interphase in lithium metal batteries. *Angew Chem Int Ed Engl* 2022;61:e202201406. DOI PubMed
50. Zheng G, Xiang Y, Chen S, et al. Additives synergy for stable interface formation on rechargeable lithium metal anodes. *Energy Storage Mater* 2020;29:377-85. DOI
51. Hagopian A, Doublet M, Filhol J. Thermodynamic origin of dendrite growth in metal anode batteries. *Energy Environ Sci* 2020;13:5186-97. DOI
52. Rosso M, Gobron T, Brissot C, Chazalviel J, Lascaud S. Onset of dendritic growth in lithium/polymer cells. *J Power Sources* 2001;97-8:804-6. DOI
53. Chen J, Li Z, Sun N, et al. A robust Li-intercalated interlayer with strong electron withdrawing ability enables durable and high-rate Li metal anode. *ACS Energy Lett* 2022;7:1594-603. DOI
54. Fan L, Li S, Liu L, et al. Enabling stable lithium metal anode via 3D inorganic skeleton with superlithiophilic interphase. *Adv Energy Mater* 2018;8:1802350. DOI
55. Zhang R, Shen X, Cheng XB, Zhang Q. The dendrite growth in 3D structured lithium metal anodes: electron or ion transfer limitation? *Energy Storage Mater* 2019;23:556-65. DOI
56. Sun X, Zhang X, Ma Q, Guan X, Wang W, Luo J. Revisiting the electroplating process for lithium-metal anodes for lithium-metal batteries. *Angew Chem Int Ed Engl* 2020;59:6665-74. DOI PubMed
57. Yan K, Lu Z, Lee H, et al. Selective deposition and stable encapsulation of lithium through heterogeneous seeded growth. *Nat Energy* 2016;1:16010. DOI
58. Liu W, Lin D, Pei A, Cui Y. Stabilizing lithium metal anodes by uniform Li-ion flux distribution in nanochannel confinement. *J Am Chem Soc* 2016;138:15443-50. DOI PubMed
59. Li D, Xie C, Gao Y, Hu H, Wang L, Zheng Z. Inverted anode structure for long-life lithium metal batteries. *Adv Energy Mater* 2022;12:2200584. DOI
60. Huang S, Yang J, Ma L, et al. Effectively regulating more robust amorphous Li clusters for ultrastable dendrite-free cycling. *Adv Sci* 2021;8:e2101584. DOI PubMed PMC
61. Zhang S, Xiao S, Li D, et al. Commercial carbon cloth: an emerging substrate for practical lithium metal batteries. *Energy Storage Mater* 2022;48:172-90. DOI
62. Chen Z, Chen W, Wang H, et al. Lithiophilic anchor points enabling endogenous symbiotic Li_3N interface for homogeneous and stable lithium electrodeposition. *Nano Energy* 2022;93:106836. DOI
63. Du J, Wang W, Wan M, et al. Doctor-blade casting fabrication of ultrathin Li metal electrode for high-energy-density batteries. *Adv Energy Mater* 2021;11:2102259. DOI
64. Jiang G, Jiang N, Zheng N, et al. MOF-derived porous Co_3O_4-NC nanoflake arrays on carbon fiber cloth as stable hosts for dendrite-free Li metal anodes. *Energy Storage Mater* 2019;23:181-9. DOI
65. Chen Y, Ke X, Cheng Y, et al. Boosting the electrochemical performance of 3D composite lithium metal anodes through synergistic structure and interface engineering. *Energy Storage Mater* 2020;26:56-64. DOI
66. Zhou T, Shen J, Wang Z, et al. Regulating lithium nucleation and deposition via MOF-derived Co@C-modified carbon cloth for stable Li metal anode. *Adv Funct Mater* 2020;30:1909159. DOI
67. Shen Y, Pu Z, Zhang Y, et al. MXene/ZnO flexible freestanding film as a dendrite-free support in lithium metal batteries. *J Mater Chem A* 2022;10:17199-207. DOI
68. Wang SH, Yin YX, Zuo TT, et al. Stable Li metal anodes via regulating lithium plating/stripping in vertically aligned microchannels. *Adv Mater* 2017;29:1703729. DOI PubMed
69. Liu S, Zhao J, Li F, Zhao Y, Li G. Regulating lithium deposition behavior by electrokinetic effects in a high-zeta-potential h-BN/zinc-lithium alloy for high-performance lithium metal anodes. *J Mater Chem A* 2022;10:5221-9. DOI
70. Xu H, Li S, Zhang C, et al. Roll-to-roll prelithiation of Sn foil anode suppresses gassing and enables stable full-cell cycling of lithium ion batteries. *Energy Environ Sci* 2019;12:2991-3000. DOI
71. Fang S, Shen L, Hoefling A, et al. A mismatch electrical conductivity skeleton enables dendrite-free and high stability lithium metal anode. *Nano Energy* 2021;89:106421. DOI
72. Zhao P, Feng Y, Li T, et al. Stable lithium metal anode enabled by high-dimensional lithium deposition through a functional organic substrate. *Energy Storage Mater* 2020;33:158-63. DOI
73. Feng X, Bai Y, Liu M, et al. Untangling the respective effects of heteroatom-doped carbon materials in batteries, supercapacitors and the ORR to design high performance materials. *Energy Environ Sci* 2021;14:2036-89. DOI
74. Liu Y, Qin X, Zhang S, et al. Oxygen and nitrogen co-doped porous carbon granules enabling dendrite-free lithium metal anode. *Energy Storage Mater* 2019;18:320-7. DOI

75. Chen X, Chen XR, Hou TZ, et al. Lithiophilicity chemistry of heteroatom-doped carbon to guide uniform lithium nucleation in lithium metal anodes. *Sci Adv* 2019;5:eaau7728. DOI PubMed PMC
76. Feng X, Wu H, Gao B, Świętosławski M, He X, Zhang Q. Lithiophilic N-doped carbon bowls induced Li deposition in layered graphene film for advanced lithium metal batteries. *Nano Res* 2022;15:352-60. DOI
77. Ge J, Hong J, Liu T, Wang Y. Rational design of a self-supporting skeleton decorated with dual lithiophilic Sn-containing and N-doped carbon tubes for dendrite-free lithium metal anodes. *J Mater Chem A* 2022;10:11458-69. DOI
78. Zhang R, Chen XR, Chen X, et al. Lithiophilic sites in doped graphene guide uniform lithium nucleation for dendrite-free lithium metal anodes. *Angew Chem Int Ed Engl* 2017;56:7764-8. DOI PubMed
79. Liu L, Yin YX, Li JY, Wang SH, Guo YG, Wan LJ. Uniform lithium nucleation/growth induced by lightweight nitrogen-doped graphitic carbon foams for high-performance lithium metal anodes. *Adv Mater* 2018;30:1706216. DOI PubMed
80. Lyu Z, Lim GJ, Guo R, et al. 3D-printed electrodes for lithium metal batteries with high areal capacity and high-rate capability. *Energy Storage Mater* 2020;24:336-42. DOI
81. Liu K, Li Z, Xie W, et al. Oxygen-rich carbon nanotube networks for enhanced lithium metal anode. *Energy Storage Mater* 2018;15:308-14. DOI
82. Li K, Hu Z, Ma J, Chen S, Mu D, Zhang J. A 3D and stable lithium anode for high-performance lithium-iodine batteries. *Adv Mater* 2019;31:e1902399. DOI PubMed
83. Xu Z, Xu L, Xu Z, Deng Z, Wang X. N, O-codoped carbon nanosheet array enabling stable lithium metal anode. *Adv Funct Mater* 2021;31:2102354. DOI
84. Li D, Zhang S, Zhang Q, et al. Pencil-drawing on nitrogen and sulfur co-doped carbon paper: an effective and stable host to pre-store Li for high-performance lithium-air batteries. *Energy Storage Mater* 2020;26:593-603. DOI
85. Xie Y, Zhang H, Yu J, et al. A novel dendrite-free lithium metal anode via oxygen and boron codoped honeycomb carbon skeleton. *Small* 2022;18:e2104876. DOI PubMed
86. Yang Z, Dang Y, Zhai P, et al. Single-atom reversible lithiophilic sites toward stable lithium anodes. *Adv Energy Mater* 2022;12:2103368. DOI
87. Zhai P, Wang T, Yang W, et al. Lithium metal anodes: uniform lithium deposition assisted by single-atom doping toward high-performance lithium metal anodes. *Adv Energy Mater* 2019;9:1804019. DOI
88. Liu H, Chen X, Cheng XB, et al. Lithium metal anodes: uniform lithium nucleation guided by atomically dispersed lithiophilic CoN*x* sites for safe lithium metal batteries. *Small Methods* 2019;3:1800354. DOI
89. Wang Y, Tan J, Li Z, et al. Recent progress on enhancing the Lithiophilicity of hosts for dendrite-free lithium metal batteries. *Energy Storage Mater* 2022;53:156-82. DOI
90. Liu Y, Lin D, Liang Z, Zhao J, Yan K, Cui Y. Lithium-coated polymeric matrix as a minimum volume-change and dendrite-free lithium metal anode. *Nat Commun* 2016;7:10992. DOI
91. Liu Y, Sun J, Hu X, et al. Lithiophilic sites dependency of lithium deposition in Li metal host anodes. *Nano Energy* 2022;94:106883. DOI
92. Wu S, Zhang Z, Lan M, et al. Lithiophilic Cu-CuO-Ni hybrid structure: advanced current collectors toward stable lithium metal anodes. *Adv Mater* 2018;30:1705830. DOI PubMed
93. Zhang C, Lv W, Zhou G, et al. Vertically aligned lithiophilic CuO nanosheets on a Cu collector to stabilize lithium deposition for lithium metal batteries. *Adv Energy Mater* 2018;8:1703404. DOI
94. Mei Y, Zhou J, Hao Y, et al. High-lithiophilicity host with micro/nanostructured active sites based on wenzel wetting model for dendrite-free lithium metal anodes. *Adv Funct Mater* 2021;31:2106676. DOI
95. Zhang Q, Bai W, Sun C, Liu X, Wang K, Chen J. Surface modification of Ni foam for stable and dendrite-free lithium deposition. *Chem Eng J* 2021;405:127022. DOI
96. Chen Y, Xu X, Gao L, et al. Two birds with one stone: using indium oxide surficial modification to tune inner helmholtz plane and regulate nucleation for dendrite-free lithium anode. *Small Methods* 2022;6:e2200113. DOI PubMed
97. Xu Y, Zheng H, Yang H, et al. Thermodynamic regulation of dendrite-free Li plating on Li_3Bi for stable lithium metal batteries. *Nano Lett* 2021;21:8664-70. DOI PubMed
98. Tabassum H, Zou R, Mahmood A, et al. A universal strategy for hollow metal oxide nanoparticles encapsulated into B/N co-doped graphitic nanotubes as high-performance lithium-ion battery anodes. *Adv Mater* 2018;30:1705441. DOI PubMed
99. Zheng J, Zhang W, Zhang J, et al. Recent advances in nanostructured transition metal nitrides for fuel cells. *J Mater Chem A* 2020;8:20803-18. DOI
100. Lei M, Wang JG, Ren L, et al. Highly lithiophilic cobalt nitride nanobrush as a stable host for high-performance lithium metal anodes. *ACS Appl Mater Interfaces* 2019;11:30992-8. DOI
101. Xu R, Zhou Y, Tang X, et al. Nanoarray architecture of ultra-lithiophilic metal nitrides for stable lithium metal anodes. *Small* 2023;19:e2205709. DOI
102. Luo L, Li J, Yaghoobnejad Asl H, Manthiram A. A 3D lithiophilic Mo_2N-modified carbon nanofiber architecture for dendrite-free lithium-metal anodes in a full cell. *Adv Mater* 2019;31:e1904537. DOI PubMed
103. Shen X, Shi S, Li B, et al. Lithiophilic interphase porous buffer layer toward uniform nucleation in lithium metal anodes. *Adv Funct Mater* 2022;32:2206388. DOI
104. Lin K, Qin X, Liu M, et al. Ultrafine titanium nitride sheath decorated carbon nanofiber network enabling stable lithium metal

anodes. *Adv Funct Mater* 2019;29:1903229. DOI

105. Fu X, Duan H, Zhang L, Hu Y, Deng Y. A 3D framework with an in situ generated Li_3N solid electrolyte interphase for superior lithium metal batteries. *Adv Funct Mater* 2023;33:2308022. DOI
106. Lee D, Sun S, Kwon J, et al. Copper nitride nanowires printed Li with stable cycling for Li metal batteries in carbonate electrolytes. *Adv Mater* 2020;32:e1905573. DOI PubMed
107. Zhang S, Yang G, Liu Z, et al. Phase diagram determined lithium plating/stripping behaviors on lithiophilic substrates. *ACS Energy Lett* 2021;6:4118-26. DOI
108. Jin S, Ye Y, Niu Y, et al. Solid-solution-based metal alloy phase for highly reversible lithium metal anode. *J Am Chem Soc* 2020;142:8818-26. DOI PubMed
109. Yang T, Li L, Wu F, Chen R. A soft lithiophilic graphene aerogel for stable lithium metal anode. *Adv Funct Mater* 2020;30:2002013. DOI
110. Zheng H, Zhang Q, Chen Q, et al. 3D lithiophilic-lithiophobic-lithiophilic dual-gradient porous skeleton for highly stable lithium metal anode. *J Mater Chem A* 2020;8:313-22. DOI
111. Li W, Luo P, Chen M, et al. Hedging Li dendrite formation by virtue of controllable tip effect. *J Mater Chem A* 2022;10:15161-8. DOI
112. Li L, Fu H, Yang J, et al. A dual-confined lithium nucleation and growth design enables dendrite-free lithium metal batteries. *J Mater Chem A* 2022;10:11659-66. DOI
113. Gao P, Wu H, Zhang X, et al. Optimization of magnesium-doped lithium metal anode for high performance lithium metal batteries through modeling and experiment. *Angew Chem Int Ed Engl* 2021;60:16506-13. DOI PubMed
114. Xu Y, Zhao S, Zhou G, et al. Solubility-dependent protective effects of binary alloys for lithium anode. *ACS Appl Energy Mater* 2020;3:2278-84. DOI
115. Liang Z, Lin D, Zhao J, et al. Composite lithium metal anode by melt infusion of lithium into a 3D conducting scaffold with lithiophilic coating. *Proc Natl Acad Sci U S A* 2016;113:2862-7. DOI PubMed PMC
116. Wan M, Kang S, Wang L, et al. Mechanical rolling formation of interpenetrated lithium metal/lithium tin alloy foil for ultrahigh-rate battery anode. *Nat Commun* 2020;11:829. DOI PubMed PMC
117. Zhou Y, Zhang J, Zhao K, et al. A novel dual-protection interface based on gallium-lithium alloy enables dendrite-free lithium metal anodes. *Energy Stor Mater* 2021;39:403-11. DOI
118. Liu Y, Qin X, Liu F, et al. Basal nanosuit of graphite for high-energy hybrid Li batteries. *ACS Nano* 2020;14:1837-45. DOI PubMed
119. Pu J, Li J, Shen Z, et al. Interlayer lithium plating in Au nanoparticles pillared reduced graphene oxide for lithium metal anodes. *Adv Funct Mater* 2018;28:1804133. DOI
120. Chen J, Xiang J, Chen X, Yuan L, Li Z, Huang Y. Li_2S-based anode-free full batteries with modified Cu current collector. *Energy Storage Mater* 2020;30:179-86. DOI
121. Zhao Z, Soni S, Lee T, Nijhuis CA, Xiang D. Smart eutectic gallium-indium: from properties to applications. *Adv Mater* 2023;35:e2203391. DOI PubMed
122. Zhou J, Qian T, Wang Z, et al. Healable lithium alloy anode with ultrahigh capacity. *Nano Lett* 2021;21:5021-7. DOI
123. Li H, Yamaguchi T, Matsumoto S, et al. Circumventing huge volume strain in alloy anodes of lithium batteries. *Nat Commun* 2020;11:1584. DOI PubMed PMC
124. Sun B, Zhang Q, Xu W, et al. A gradient topology host for a dendrite-free lithium metal anode. *Nano Energy* 2022;94:106937. DOI
125. Wu J, Ju Z, Zhang X, et al. Gradient design for high-energy and high-power batteries. *Adv Mater* 2022;34:e2202780. DOI PubMed
126. Le T, Liang Q, Chen M, et al. Lithium metal anodes: a triple-gradient host for long cycling lithium metal anodes at ultrahigh current density (small 30/ 2020). *Small* 2020;16:e2001992. DOI
127. Guo W, Liu S, Guan X, Zhang X, Liu X, Luo J. Mixed ion and electron-conducting scaffolds for high-rate lithium metal anodes. *Adv Energy Mater* 2019;9:1900193. DOI
128. Li J, Zou P, Chiang SW, et al. A conductive-dielectric gradient framework for stable lithium metal anode. *Energy Storage Mater* 2020;24:700-6. DOI
129. Zhou S, Fu C, Chang Z, et al. Conductivity gradient modulator induced highly reversible Li anodes in carbonate electrolytes for high-voltage lithium-metal batteries. *Energy Storage Mater* 2022;47:482-90. DOI
130. Nan Y, Li S, Shi Y, Yang S, Li B. Gradient-distributed nucleation seeds on conductive host for a dendrite-free and high-rate lithium metal anode. *Small* 2019;15:e1903520. DOI PubMed
131. Lv Y, Zhang Q, Li C, et al. Bottom-up Li deposition by constructing a multiporous lithiophilic gradient layer on 3D Cu foam for stable Li metal anodes. *ACS Sustainable Chem Eng* 2022;10:7188-95. DOI
132. Li T, Gu S, Chen L, et al. Bidirectional lithiophilic gradients modification of ultralight 3D carbon nanofiber host for stable lithium metal anode. *Small* 2022;18:e2203273. DOI
133. Huang S, Zhang H, Fan LZ. Confined lithium deposition triggered by an integrated gradient scaffold for a lithium-metal anode. *ACS Appl Mater Interfaces* 2022;14:17539-46. DOI PubMed
134. Yu Z, Yang Q, Xue W, et al. Uniformizing the lithium deposition by gradient lithiophilicity and conductivity for stable lithium-metal batteries. *Nanoscale* 2023;15:4529-35. DOI
135. Hong SH, Jung DH, Kim JH, et al. Electrical conductivity gradients: electrical conductivity gradient based on heterofibrous scaffolds

for stable lithium-metal batteries. *Adv Funct Mater* 2020;30:1908868. DOI

136. Pu J, Li J, Zhang K, et al. Conductivity and lithiophilicity gradients guide lithium deposition to mitigate short circuits. *Nat Commun* 2019;10:1896. DOI PubMed PMC
137. Yun J, Park B, Won E, et al. Bottom-up lithium growth triggered by interfacial activity gradient on porous framework for lithium-metal anode. *ACS Energy Lett* 2020;5:3108-14. DOI
138. Liu H, Di J, Wang P, et al. A novel design of 3D carbon host for stable lithium metal anode. *Carbon Energy* 2022;4:654-64. DOI
139. Pan J, Shi K, Wu H, et al. Lithium dredging and capturing dual-gradient framework enabling step-packed deposition for dendrite-free lithium metal anodes. *Adv Energy Mater* 2024;14:2302862. DOI
140. Wang D, Liu H, Liu F, et al. Phase-separation-induced porous lithiophilic polymer coating for high-efficiency lithium metal batteries. *Nano Lett* 2021;21:4757-64. DOI
141. Jiang J, Pan Z, Kou Z, et al. Lithiophilic polymer interphase anchored on laser-punched 3D holey Cu matrix enables uniform lithium nucleation leading to super-stable lithium metal anodes. *Energy Storage Mater* 2020;29:84-91. DOI
142. Li NW, Shi Y, Yin YX, et al. A flexible solid electrolyte interphase layer for long-life lithium metal anodes. *Angew Chem Int Ed Engl* 2018;57:1505-9. DOI PubMed